Second order nonlinear spatial stability analysis of compressible mixing layers

F. Ladeinde and J. Wu
Department of Mechanical Engineering, SUNY at Stony Brook, Stony Brook, New York 11794-2300

(Received 3 December 2001; accepted 17 May 2002; published 2 August 2002)

Second order nonlinear spatial stability to three-dimensional perturbation waves is analyzed for compressible mixing layers by expanding the perturbations into amplitude-dependent harmonic waves and truncating the Landau equation to the second term. This leads to a system of nonlinear ordinary differential equations for the harmonics. The two constants in Landau equation are calculated, wherein the independent variable, time *t*, is replaced by the streamwise coordinate direction *x*. The basic procedure in this paper is similar to that by Liu for compressible laminar wakes [Phys. Fluids **12**, 1763 (1969)]. However, unlike this reference, which does not provide any results for their analysis, the present paper obtained many interesting results. The linear results from the present work compare very favorably with those reported by Day, Reynolds, and Mansour [Phys. Fluids **10**, 993 (1998)], who employed a different procedure and limited their analysis to the linear regime. In the present studies, both the linear and nonlinear problems were analyzed in exactly the same manner, with the implication that the nonlinear results are probably accurate. These results include the convergence of the amplitude to an equilibrium value that depends on the two constants in the amplitude equation from Landau's procedure. The present analysis is restricted to exponentially decaying linear solutions at the boundaries and hence to region one in the phase speed-Mach number diagram. However, we have observed that nonlinear effects could introduce constant, decaying, or outgoing wave solutions at the boundaries, depending on the velocity and density ratios and the Mach number of the fast stream. Other effects of these parameters are reported. © *2002 American Institute of Physics.* [DOI: 10.1063/1.1492284]

I. INTRODUCTION

Mixing layers are often used to model some natural phenomena and engineering devices such as combustors and gas lasers. Figure 1 is a schematic of the flow structure in mixing layers, which are formed by the merging of two streams that are initially separated by a thin splitter plate. The streams could have different velocities, densities, and temperatures. Due to the high shear between the streams, intense mixing occurs in the velocity-gradient region, which is of great importance in industrial applications. For example, the combustion mixing layer model of the scramjet propulsion concept requires rapid mixing between fuel and air in order to minimize the size of the combustor. A detailed understanding of the stability characteristics is needed to properly analyze mixing enhancement. Besides, the stability results could also be used to generate initial conditions for numerical simulations.

The linear stability analysis of both the temporal and spatial waves has received some attention (Michalke[1–3]) while the characteristics of large coherent structures have been investigated by Brown and Roshko[4] in their experimental study of mixing layers. They discussed the central instability mode for two-dimensional incompressible, nonreacting flows. Lesson, Fox, and Zien[5] analyzed the inviscid temporal stability of compressible mixing layers that were subjected to two-dimensional and three-dimensional disturbances. The spatial case was investigated by Goldstein and Leib,[6] Grosch and Jackson,[7] and Jackson and Grosch.[8] In addition to the central mode, they also reported on the two outer modes. The outer modes were further investigated by Day, Reynolds, and Mansour,[9] hereafter referred to as DRM, in studies that were extended to the reacting case. The combined effects of compressibility, heat release, density ratio, equivalence ratio, and velocity ratio on the instability characteristics of each mode were also discussed. Planché and Reynolds[10] observed that heating favored the outer instability modes in linear, small amplitude disturbance theory. Ragab and Wu[11] examined the viscous and inviscid stability of a compressible mixing layer using both the hyperbolic tangent profile and Sutherland viscosity profiles. They found that the disturbances could be calculated very accurately from the inviscid theory if the Reynolds number, Re, is greater than 1000. (The inviscid results yield the upper bound for the growth rate since viscosity damps out the perturbations.) In addition, Ragab and Wu reported that nonparallel effects were negligible. The studies by Schade[12] also showed that viscosity did not have a destabilizing effect in an unbounded flow. The effects of compressibility on instability has been studied,[9,13,16] subsequent to the work of Papamoschou and Roshko,[14] which suggested the use of ''convective Mach number'' to study compressibility effects on mixing layers. The general result is that compressibility enhances stability at low to moderate

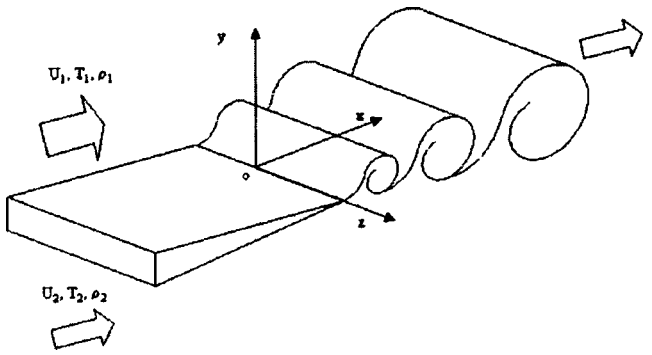

FIG. 1. Schematic of the flow structures.

Mach numbers, while three-dimensional characteristics evolve at higher Mach numbers.

A procedure that is often used to study stability, for example in Ladeinde and Torrance,[15] consists of an exact, closed-form analysis for the linear problem followed by a purely numerical calculation of the nonlinear or finite amplitude components. Although this procedure allows the computation of very strong flows, complete details of the departure from linearity, which are often of interest, cannot be obtained from such methods. In the present work, both the linear and nonlinear problems are analyzed using the Landau's procedure which, although being limited to weak nonlinearities, provides invaluable results on the evolution of the perturbation into the nonlinear regime. Compared to the linear case, an additional model is needed to close the nonlinear system in the form of the Landau equation. The application of this equation for the analysis of other problems has been reported. Stuart[17] derived the equation from the energy equation in rotational Couette flow while Palm[18] investigated Bénard convection. The plane parallel flow problem was analyzed by Stuart[19] and Watson,[20] which led to subsequent applications to the circular Couette flow and plane Poiseuille flows. Eagles[21] studied the stability of Taylor vortices by fifth-order amplitude expansions and proposed a method for the determination of the Landau constant. Finally, Liu[22] analyzed the weakly nonlinear instability of compressible laminar wake, using an approach that is similar to the one in the present paper. However, his study was inconclusive since no results were presented.

It should be noted that for strong departure from the linear regime, such as critical-layer type instability,[6,23–25] the method of matched asymptotic expansion may be more appropriate. In this case, the perturbed shear layer is divided into two overlapped domains, with the same governing equations in each domain but different transverse length scales. This is not the focus of the present work. From weak to moderate level of nonlinearity, this paper presents the effects of convective Mach number, velocity and density ratios and extends the nonreacting results in DRM from the linear to the nonlinear regime.

Section II of the paper presents the governing equations, followed by the Landau's approach in Sec. III. The decomposition of the flow variables, the governing equations for the linear and nonlinear components, and the solution of these equations are also described in Sec. III. Results are presented in Sec. IV.

II. GOVERNING EQUATIONS

A schematic of the mixing layers is shown in Fig. 1, where x, y, and z are defined as the streamwise, normal and spanwise coordinate directions. The dependent variables ρ, u, v, w, T, and p are the density, velocities in the x, y, z directions, temperature, and pressure, respectively. In the following, the quantities with subscript 1 refer to the fast stream, while those with subscript 2 are for the slow stream.

The models are governed by the nondimensional continuity, Euler, and energy equations:

$$\frac{\partial \rho}{\partial t}+\frac{\partial(\rho u_i)}{\partial x_i}=0, \tag{1}$$

$$\rho\frac{\partial u_i}{\partial t}+\rho u_j\frac{\partial u_i}{\partial x_j}=-\frac{\partial p}{\partial x_i}, \tag{2}$$

$$\rho\frac{\partial T}{\partial t}+\rho u_i\frac{\partial T}{\partial x_i}=-\gamma M_1^2(\gamma-1)p\frac{\partial u_i}{\partial x_i}. \tag{3}$$

The equation of state can be written as

$$p=\frac{1}{\gamma M_1^2}\cdot\rho T, \tag{4}$$

where M_1 is the Mach number of the fast stream.

Nondimensional quantities are introduced as follows:

$$\begin{aligned} &u_i=\frac{u_i^*}{U_1^*},\quad \rho=\frac{\rho^*}{\rho_1^*},\quad T=\frac{T^*}{T_1^*},\\ &p=\frac{p^*}{\rho_1^* U_1^{*2}},\quad x_i=\frac{x_i^*}{\delta_{w0}^*},\quad t=\frac{t^*}{\delta_{w0}^*/U_1^*}, \end{aligned} \tag{5}$$

where the superscript "*" denotes dimensional quantities and

$$\delta_{w0}^*=\frac{U_1^*-U_2^*}{\left|\frac{d\bar{u}^*}{dy^*}\right|_{\max}} \tag{6}$$

is the vorticity thickness of the initial velocity profile. In this paper r and s are used to denote the velocity and density ratios: $r=U_2/U_1$, $s=\rho_2/\rho_1$.

III. STABILITY ANALYSIS

Landau equation serves as the model for amplitude development, either in time or space, depending on the nature of the flow. It will be assumed that the base flow is locally parallel, with negligible velocities in the y and z coordinate directions, and that the pressure is spatially uniform. The disturbances are of the parallel type and inviscid, with amplitudes that are small compared to the base flow. The base velocity is specified either as hyperbolic tangent:

$$\overline{u}(y)=\frac{1+U_2}{2}+\frac{1-U_2}{2}\tanh(2y), \tag{7}$$

or as the self-similar solution of the compressible boundary layer equation. In either case, the temperature is obtained from the Crocco–Busemann relation:

$$\overline{T}=M_1^2\frac{(\gamma-1)}{2}(\overline{u}(1+U_2)-\overline{u^2}-U_2)+\frac{T_2(1-\overline{u})}{1-U_2}+\frac{(\overline{u}-U_2)}{1-U_2}. \tag{8}$$

The uniform pressure value is $1/\gamma M_1^2$, U_2, and T_2 are the nondimensional velocity and temperature of the slow stream and γ is the ratio of the specific heats. Density is obtained as $1/T$.

A. Nonlinear stability equations

To obtain the nonlinear stability equations, the dimensionless perturbation waves are expanded in Fourier series in time. Using density as an example, the expansion takes the form

$$\rho(x,y,z,t)=\rho_0(y,A)+\sum_{n=1}^{\infty}[\rho_n(y,A)e^{ni(\beta z-\omega t)}+\tilde{\rho}_n(y,A)e^{-ni(\beta z-\omega t)}], \tag{9}$$

where $\tilde{\rho}_n(y,A)$ is the complex conjugate of $\rho_n(y,A)$ and A is the complex amplitude. The following expansion is introduced, following Watson[20,29] and Stuart:[28]

$$\rho_n(y,A)=\sum_{m=0}^{\infty}\rho_{nm}(y)A^n|A|^{2m}. \tag{10}$$

The series for amplitude A uses the Landau equation for closure which, for the present spatial problem, can be written as

$$\frac{dA}{dx}=A(i\alpha+a_1|A|^2+O(|A|^4)). \tag{11}$$

This equation also leads to the following:

$$\frac{d\tilde{A}}{dx}=\tilde{A}(-i\tilde{\alpha}+\tilde{\alpha}_1|A|^2+O(|A|^4)), \tag{12}$$

$$\frac{d|A|^2}{dx}=\tilde{A}\frac{dA}{dx}+A\frac{d\tilde{A}}{dx}=|A|^2(-2\alpha_I+2a_{1R}|A|^2+O(|A|^4)), \tag{13}$$

where A, α, and a_1 are complex quantities. Note that the linear problem retains only the first term on the right-hand side of this equation. Equation (9) can easily be written as

$$\begin{aligned}\rho=&\rho_{00}(y)+\rho_{01}(y)|A(x)|^2+\rho_{10}(y)A(x)e^{i(\beta z-\omega t)}\\&+\tilde{\rho}_{10}(y)\tilde{A}(x)e^{-i(\beta z-\omega t)}+\rho_{11}(y)|A(x)|^2\\&\times A(x)e^{i(\beta z-\omega t)}+\tilde{\rho}_{11}(y)|A(x)|^2\tilde{A}(x)e^{-i(\beta z-\omega t)}\\&+\rho_{20}(y)A(x)^2e^{2i(\beta z-\omega t)}+\tilde{\rho}_{20}(y)\tilde{A}(x)^2e^{-2i(\beta z-\omega t)}\\&+\cdots,\end{aligned} \tag{14}$$

where "~" denotes complex conjugate.

The other dependent variables can be expanded in a similar fashion, leading to the following vector representation for the various dependent variables:

$$\begin{aligned}\mathbf{V}=(\rho,u,v,w,T,p)^T=&(\rho_{00},u_{00},v_{00},w_{00},T_{00},p_{00})^T+(\rho_{01},u_{01},v_{01},w_{01},T_{01},p_{01})^T|A(x)|^2\\&+(\rho_{10},u_{10},v_{10},w_{10},T_{10},p_{10})^TA(x)e^{i(\beta z-\omega t)}+(\tilde{\rho}_{10},\tilde{u}_{10},\tilde{v}_{10},\tilde{w}_{10},\tilde{T}_{10},\tilde{p}_{10})^T\tilde{A}(x)e^{-i(\beta z-\omega t)}\\&+(\rho_{20},u_{20},v_{20},w_{20},T_{20},p_{20})^TA(x)^2e^{2i(\beta z-\omega t)}+(\tilde{\rho}_{20},\tilde{u}_{20},\tilde{v}_{20},\tilde{w}_{20},\tilde{T}_{20},\tilde{p}_{20})^T\tilde{A}(x)^2e^{-2i(\beta z-\omega t)}\\&+(\rho_{11},u_{11},v_{11},w_{11},T_{11},p_{11})^TA(x)|A(x)|^2e^{i(\beta z-\omega t)}+(\tilde{\rho}_{11},\tilde{u}_{11},\tilde{v}_{11},\tilde{w}_{11},\tilde{T}_{11},\tilde{p}_{11})^T\tilde{A}(x)|A(x)|^2e^{-i(\beta z-\omega t)}.\end{aligned} \tag{15}$$

We also define

$$\mathbf{V}_{nm}=(\rho_{nm},u_{nm},v_{nm},w_{nm},T_{nm},p_{nm})^T, \tag{16}$$

where, for example,

$$\rho_{nm}=\rho_{00},\rho_{01},\rho_{10},\ldots. \tag{17}$$

The governing equations for the perturbations can be obtained by inserting the Fourier expansions into the continuity, momentum, energy, and state equations and collecting the like terms. Using Eq. (15) and retaining the coefficients of $A(x)e^{i(\beta z-\omega t)}$, the linear problem can be written as

$$\mathbb{M}_{10}\mathbf{V}_{10}=\mathbf{0}, \tag{18}$$

where

$$\mathbb{M}_{10}=\begin{pmatrix} i(\alpha u_{00}-\omega) & i\alpha\rho_{00} & \frac{d\rho_{00}}{dy}+\rho_{00}D & i\beta\rho_{00} & 0 & 0 \\ 0 & i(\alpha u_{00}-\omega)\rho_{00} & \rho_{00}\frac{du_{00}}{dy} & 0 & 0 & i\alpha \\ 0 & 0 & i(\alpha u_{00}-\omega)\rho_{00} & 0 & 0 & D \\ 0 & 0 & 0 & i(\alpha u_{00}-\omega)\rho_{00} & 0 & i\beta \\ 0 & (\gamma-1)i\alpha & \rho_{00}\frac{dT_{00}}{dy}+(\gamma-1)D & (\gamma-1)i\beta & i(\alpha u_{00}-\omega)\rho_{00} & 0 \\ \frac{1}{\gamma M_1^2}T_{00} & 0 & 0 & 0 & \frac{1}{\gamma M_1^2}\rho_{00} & -1 \end{pmatrix} \tag{19}$$

and $D\equiv d/dy$.

The equations in (18) constitute an eigenvalue problem, with α as the eigenvalue. In a given base flow configuration with a fixed Mach number, velocity ratio, and density ratio, disturbance waves of various frequency ω and oblique angle $\theta\equiv\tan^{-1}\beta/\alpha_r$ are possible. However, only one of these will have the largest growth rate $-\alpha_{I\,\max}$. In order to find $-\alpha_{I\,\max}$, it is necessary to search across the whole (ω, θ) plane. DRM found that the most unstable wave has a frequency less than 1 and an oblique angle $\theta\approx 56°$. We have therefore restricted our search to be within $0.0\leqslant\omega\leqslant 2.0$ and $0°\leqslant\theta\leqslant 85°$.

Equating the terms containing $|A(x)|^2$ yields the governing equations for the nonlinear part ϕ_{01},

$$\mathbb{M}_{01}\mathbf{V}_{01}=\mathbf{f}_{01}, \tag{20}$$

where

$$\mathbb{M}_{01}=\begin{pmatrix} -2\alpha_I u_{00} & -2\alpha_I\rho_{00} & \frac{d\rho_{00}}{dy}+\rho_{00}D & 0 & 0 & 0 \\ 0 & -2\alpha_I\rho_{00}u_{00} & \rho_{00}\frac{du_{00}}{dy} & 0 & 0 & -2\alpha_I \\ 0 & 0 & -2\alpha_I\rho_{00}u_{00} & 0 & 0 & -D \\ 0 & 0 & 0 & -2\alpha_I\rho_{00}u_{00} & 0 & 0 \\ 0 & -(\gamma-1)2\alpha_I & \rho_{00}\frac{dT_{00}}{dy}+(\gamma-1)D & 0 & -2\alpha_I\rho_{00}u_{00} & 0 \\ \frac{1}{\gamma M_1^2}T_{00} & 0 & 0 & 0 & \frac{1}{\gamma M_1^2}\rho_{00} & -1 \end{pmatrix}. \tag{21}$$

The source vector $\mathbf{f}_{01}$ is defined in the Appendix. Note that ω and β do not appear in these equations. The terms containing $A(x)^2e^{2i(\beta z-\omega t)}$ give the governing equations for the nonlinear part ϕ_{20},

$$\mathbb{M}_{20}\mathbf{V}_{20}=\mathbf{f}_{20}, \tag{22}$$

where

$$\mathbb{M}_{20}=\begin{pmatrix} 2i(\alpha u_{00}-\omega) & 2i\alpha\rho_{00} & \frac{d\rho_{00}}{dy}+\rho_{00}D & 2i\beta\rho_{00} & 0 & 0 \\ 0 & 2i(\alpha u_{00}-\omega)\rho_{00} & \rho_{00}\frac{du_{00}}{dy} & 0 & 0 & 2i\alpha \\ 0 & 0 & 2i(\alpha u_{00}-\omega)\rho_{00} & 0 & 0 & D \\ 0 & 0 & 0 & 2i(\alpha u_{00}-\omega)\rho_{00} & 0 & 2i\beta \\ 0 & (\gamma-1)2i\alpha & \rho_{00}\frac{dT_{00}}{dy}+(\gamma-1)D & 2(\gamma-1)i\beta & 2i(\alpha u_{00}-\omega)\rho_{00} & 0 \\ \frac{1}{\gamma M_1^2}T_{00} & 0 & 0 & 0 & \frac{1}{\gamma M_1^2}\rho_{00} & -1 \end{pmatrix}. \tag{23}$$

The source vector $\mathbf{f}_{20}$ is defined in the Appendix.

The coefficients of $|A(x)|^2\,A(x)e^{i(\beta z-\omega t)}$ lead to the governing equations for nonlinear part ϕ_{11},

$$\mathbb{M}_{11}\mathbf{V}_{11}=a_1\mathbf{f}_{10}+\mathbf{f}_{11}, \tag{24}$$

where a_1 is the Landau constant, $\alpha_3=(\alpha_r,3\alpha_I)$, and

$$\mathbb{M}_{11}=\begin{pmatrix} i(\alpha_3 u_{00}-\omega) & i\alpha_3\rho_{00} & \frac{d\rho_{00}}{dy}+\rho_{00}D & i\beta\rho_{00} & 0 & 0 \\ 0 & i(\alpha_3 u_{00}-\omega)\rho_{00} & \rho_{00}\frac{du_{00}}{dy} & 0 & 0 & i\alpha_3 \\ 0 & 0 & i(\alpha_3 u_{00}-\omega)\rho_{00} & 0 & 0 & D \\ 0 & 0 & 0 & i(\alpha_3 u_{00}-\omega)\rho_{00} & 0 & i\beta \\ 0 & (\gamma-1)i\alpha_3 & \rho_{00}\frac{dT_{00}}{dy}+(\gamma-1)D & (\gamma-1)i\beta & i(\alpha_3 u_{00}-\omega)\rho_{00} & 0 \\ \frac{1}{\gamma M_1^2}T_{00} & 0 & 0 & 0 & \frac{1}{\gamma M_1^2}\rho_{00} & -1 \end{pmatrix}, \tag{25}$$

and the source terms $\mathbf{f}_{10}$ and $\mathbf{f}_{11}$ are defined in the Appendix.

B. Solution of the perturbation equations

1. The linear part

The linear part [Eq. (18)] can be solved with the procedure developed by Gropengiesser.[30] Defining

$$\chi=\frac{i\alpha p_{10}}{v_{10}}, \tag{26}$$

the equations can be reduced to a single nonlinear, first order differential equation,

$$\chi'=\rho_{00}\alpha^2\left(u_{00}-\frac{\omega}{\alpha}\right)-\frac{\chi\left(\chi g+\frac{du_{00}}{dy}\right)}{u_{00}-\frac{\omega}{\alpha}}, \tag{27}$$

where

$$g=T_{00}\left(1+\frac{\beta^2}{\alpha^2}\right)-M_1^2\left(u_{00}-\frac{\omega}{\alpha}\right)^2. \tag{28}$$

For boundary conditions, du_{00}/dy approaches zero as $y\to\pm\infty$. The quantities u_{00}, T_{00}, ρ_{00}, and g_{10} are constant. Letting $du_{00}/dy=0$ and $\chi'=0$ gives

$$\chi(y=\pm\infty)=\mp\frac{\alpha\left(u_{00}-\frac{\omega}{\alpha}\right)}{\sqrt{gT_{00}}}. \tag{29}$$

An eigenvalue problem results from Eq. (27) with eigenvalue α. With the boundary conditions in the two free streams, Eq. (27) is integrated from $y\to\pm\infty$ to $y=0$ using the fourth order Runge–Kutta scheme. The two values of χ^+ and χ^- obtained from this procedure are compared and iterated on α until they become essentially equal at $y=0$.

2. The nonlinear part ϕ_{01}

Two coupled ordinary differential equations (ODEs) are obtained from Eq. (20):

$$\frac{dp_{01}}{dy}=2\alpha_I\rho_{00}u_{00}v_{01}+f_{01p}, \tag{30}$$

$$u_{00}\frac{dv_{01}}{dy}=\frac{du_{00}}{dy}v_{01}+2\alpha_I(M_1^2u_{00}^2-T_{00})p_{01}+f_{01v}, \tag{31}$$

with

$$f_{01p}=f_{013}, \tag{32}$$

$$f_{01v}=\frac{u_{00}}{\gamma}(T_{00}f_{011}+f_{015})+2\alpha_I M_1^2u_{00}^2f_{016}-T_{00}f_{012}. \tag{33}$$

Equations (30)–(33) are valid for all values of y. The boundary conditions are obtained by considering the behavior as $y\to\pm\infty$. The ODEs are solved numerically. In these limits, no shear exists, and all functions constructed from the base flow are independent of y. From the linear solution, the variables in ϕ_{10} have exponential tails at (both) free streams, i.e., they are of the form $Ce^{\pm q_{10}y}$, where C is a constant, so that the inhomogeneous terms have the form $C'e^{\pm 2q_{10R}y}$, where C' is another constant and q_{10R} is the real part of q_{10}. Note that the restriction to exponentially decaying ϕ_{10} values at the free streams implies that the present analysis is restricted to subsonic disturbances, and hence to region one in the phase speed-Mach number diagram.[8] However, the nonlinear problem could introduce constant, decaying, or outgoing wave solutions at the boundaries depending on M_1^2 (fast stream) or $M_1^2sr^2$ (slow stream). This is a new result, which will be discussed in more detail later in this paper.

In the limit $y\to+\infty$, Eqs. (30) and (31) can be written as

$$\frac{dp_{01}}{dy}=2\alpha_I v_{01}+B_{1p}e^{-2q_{10R}y}, \tag{34}$$

$$\frac{dv_{01}}{dy}=2\alpha_I(M_1^2-1)p_{01}+B_{2p}e^{-q_{10R}y}, \tag{35}$$

which, upon differentiating, gives

$$\frac{d^2p_{01}}{dy^2}=4\alpha_I^2(M_1^2-1)p_{01}+2(\alpha_I B_{2p}-q_{10R}B_{1p})e^{-2q_{10R}y}, \tag{36}$$

$$\frac{d^2v_{01}}{dy^2}=4\alpha_I^2(M_1^2-1)v_{01}+2[\alpha_I(M_1^2-1)B_{1p}-q_{10R}B_{2p}]e^{-2q_{10R}y}. \quad (37)$$

The general solutions of (36) and (37) depend on M_1^2 as follows.

When $M_1^2>1$ and we define $q_{01}\equiv 2|\alpha_I|\sqrt{M_1^2-1}$, the solutions of (36) and (37) are

$$p_{01}=c_1e^{-q_{01}y}+\frac{2\alpha_IB_{2p}-2q_{10R}B_{1p}}{4q_{10R}^2-q_{01}^2}e^{-2q_{10R}y}, \quad (38)$$

$$v_{01}=c_3e^{-q_{01}y}+\frac{2\alpha_I(M_1^2-1)B_{1p}-2q_{10R}B_{2p}}{4q_{10R}^2-q_{01}^2}e^{-2q_{10R}y}. \quad (39)$$

The original Eq. (34) requires that

$$\frac{c_1}{c_3}=-\frac{\mathrm{sign}(\alpha_I)}{\sqrt{M_1^2-1}}. \quad (40)$$

The solution for the sonic limit $M_1^2=1$ can be obtained as

$$p_{01}=\frac{\alpha_IB_{2p}-q_{10R}B_{1p}}{2q_{10R}^2}e^{-2q_{10R}y}+c_1, \quad (41)$$

$$v_{01}=-\frac{B_{2p}}{2q_{10R}^2}e^{-2q_{10R}y}. \quad (42)$$

When $M_1^2<1$ and we define $q_{01}\equiv 2|\alpha_I|\sqrt{1-M_1^2}$, the solutions of (36) and (37) are

$$p_{01}=c_1\cos(q_{01}y+\phi_p)+\frac{2\alpha_IB_{2p}-2q_{10R}B_{1p}}{4q_{10R}^2+q_{01}^2}e^{-2q_{10R}y}, \quad (43)$$

$$v_{01}=c_3\cos(q_{01}y+\phi_v)+\frac{2\alpha_I(M_1^2-1)B_{1p}-2q_{10R}B_{2p}}{(4q_{10R}^2+q_{01}^2)}e^{-2q_{10R}y}. \quad (44)$$

In this case, Eq. (34) requires that

$$\phi_v=\phi_p+\frac{\pi}{2}, \quad (45)$$

$$\frac{c_1}{c_3}=\frac{\mathrm{sign}(\alpha_I)}{\sqrt{1-M_1^2}}. \quad (46)$$

The solutions in the asymptotic limit $y\to-\infty$ can also be obtained in a similar fashion if we note that Eq. (30) and (31) become

$$\frac{dp_{01}}{dy}=2\alpha_Irsv_{01}+B_{1n}e^{2q_{10R}y}, \quad (47)$$

$$r\frac{dv_{01}}{dy}=2\alpha_I(M_1^2r^2-1/s)p_{01}+B_{2n}e^{q_{10R}y}, \quad (48)$$

which can be differentiated to give

$$\frac{d^2p_{01}}{dy^2}=4\alpha_I^2(M_1^2sr^2-1)p_{01}+2(\alpha_IsB_{2n}+q_{10R}B_{1n})e^{2q_{10R}y}, \quad (49)$$

$$\frac{d^2v_{01}}{dy^2}=4\alpha_I^2(M_1^2sr^2-1)v_{01}+\frac{2}{r}[\alpha_I(M_1^2r^2-1/s)B_{1n}+q_{10R}B_{2n}]e^{2q_{10R}y}. \quad (50)$$

When $M_1^2sr^2>1$ and $q_{01}\equiv 2|\alpha_I|\sqrt{M_1^2sr^2-1}$, the solutions are

$$p_{01}=c_2e^{q_{01}y}+\frac{2\alpha_IsB_{2n}+2q_{10R}B_{1n}}{2q_{10R}^2-q_{01}^2}e^{2q_{10R}y}, \quad (51)$$

$$v_{01}=c_4e^{q_{01}y}+\frac{2\alpha_I(M_1^2r^2-1/s)B_{1n}+2q_{10R}B_{2n}}{r(2q_{10R}^2-q_{01}^2)}e^{2q_{10R}y}, \quad (52)$$

where

$$\frac{c_2}{c_4}=\frac{\mathrm{sign}(\alpha_I)rs}{\sqrt{M_1^2sr^2-1}}. \quad (53)$$

The solutions for $M_1^2sr^2=1$ are

$$p_{01}=\frac{\alpha_IsB_{2n}+q_{10R}B_{1n}}{2q_{10R}^2}e^{2q_{10R}y}+c_2, \quad (54)$$

$$v_{01}=\frac{B_{2n}}{2rq_{10R}^2}e^{2q_{10R}y}. \quad (55)$$

For $M_1^2sr^2<1$ and $q_{01}\equiv 2|\alpha_I|\sqrt{1-M_1^2sr^2}$:

$$p_{01}=c_2\cos(q_{01}y+\phi_p)+\frac{2\alpha_IsB_{2n}+2q_{10R}B_{1n}}{4q_{10R}^2+q_{01}^2}e^{2q_{10R}y}, \quad (56)$$

$$v_{01}=c_4\cos(q_{01}y+\phi_v)+\frac{2\alpha_I(M_1^2r^2-1/s)B_{1n}+2q_{10R}B_{2n}}{r(4q_{10R}^2+q_{01}^2)}e^{2q_{10R}y}, \quad (57)$$

where

$$\phi_v=\phi_p+\frac{\pi}{2}, \quad (58)$$

$$\frac{c_2}{c_4}=\frac{\mathrm{sign}(\alpha_I)rs}{\sqrt{1-M_1^2sr^2}}. \quad (59)$$

3. The nonlinear part ϕ_{20}

The nonlinear part [Eq. (22)] can be written as a set of coupled equations

$$\frac{dv_{20}}{dy}=\frac{\frac{du_{00}}{dy}}{u_{00}-\frac{\omega}{\alpha}}v_{20}+\frac{2i\alpha g}{u_{00}-\frac{\omega}{\alpha}}p_{20}+f_{20v}, \quad (60)$$

$$\frac{dp_{20}}{dy}=-\rho_{00}2i\alpha\left(u_{00}-\frac{\omega}{\alpha}\right)v_{20}+f_{20p}, \tag{61}$$

where

$$f_{20p}=f_{203}, \tag{62}$$

$$f_{20v}=\frac{T_{00}f_{201}+f_{205}}{\gamma}-2i(\alpha u_{00}-\omega)M_1^2 f_{206}-\frac{\alpha f_{202}+\beta f_{204}}{\rho_{00}(\alpha u_{00}-\omega)}. \tag{63}$$

The boundary conditions for these equations can be obtained from the linear part, from which we know that the variables have exponential tails at (both) free streams and can be represented in the form $Ce^{\pm q_{10}y}$, where C is a constant. Each of the inhomogeneous terms appearing in these governing equations is the sum of products, such as $\phi_{10}\psi_{10}$ and so behaves as $C'e^{\pm 2q_{10}y}$, where C' is a constant. Therefore, as $y\to\pm\infty$ and $du_{00}/dy=0$, the equations simplify to

$$\frac{dv_{20}}{dy}=\frac{2i\alpha g}{u_{00}-\frac{\omega}{\alpha_0}}p_{20}+B_1e^{\pm 2q_{10}y}, \tag{64}$$

$$\frac{dp_{20}}{dy}=-\rho_{00}2i\alpha\left(u_{00}-\frac{\omega}{\alpha}\right)v_{20}+B_2e^{\pm 2q_{10}y}. \tag{65}$$

The variables in these equations are constant except v_{20}, p_{20} and the "y" in $e^{\pm 2q_{10}y}$. The exponential behavior of the inhomogeneous terms suggests solutions in the form

$$v_{20}(y)=c_v(y)e^{\pm 2q_{10}y}, \tag{66}$$

$$p_{20}(y)=c_p(y)e^{\pm 2q_{10}y}. \tag{67}$$

Substituting back into Eqs. (64) and (65) and requiring finite values at $y\to\pm\infty$, we obtain the following system of boundary conditions at the upper half of the layer:

$$2q_{10}c_1+\frac{2i\alpha g}{1-\frac{\omega}{\alpha}}c_3=-\frac{i\alpha g}{1-\frac{\omega}{\alpha}}\frac{B_{2p}}{2q_{10}}-\frac{B_{1p}}{2}, \tag{68}$$

$$v_{20}=\left(c_1-\frac{i\alpha gB_{2p}}{2q_{10}\left(1-\frac{\omega}{\alpha}\right)}y+\frac{B_{1p}}{2}y\right)e^{-2q_{10}y}, \tag{69}$$

$$p_{20}=\left(c_3+i\alpha\left(1-\frac{\omega}{\alpha}\right)\frac{B_{1p}}{2q_{10}}y+\frac{B_{2p}}{2}y\right)e^{-2q_{10}y}, \tag{70}$$

where we have used the fact that $u_{00}=1$ at this boundary.

The analogous equations for the lower half of the layer are

$$2q_{10}c_2-\frac{2i\alpha g}{r-\frac{\omega}{\alpha}}c_4=\frac{B_{1n}}{2}-\frac{i\alpha g}{r-\frac{\omega}{\alpha}}\frac{B_{2n}}{2q_{10}}, \tag{71}$$

$$v_{20}\left(y\to-\infty,\frac{dr}{dy}=0\right)=\left(c_2+\frac{i\alpha g}{r-\frac{\omega}{\alpha}}\frac{B_{2n}}{2q_{10}}y+\frac{B_{1n}}{2}y\right)e^{2q_{10}y}, \tag{72}$$

$$p_{20}\left(y\to-\infty,\frac{dr}{dy}=0\right)=\left(c_4-si\alpha\left(r-\frac{\omega}{\alpha}\right)\frac{B_{1n}}{2q_{10}}y+\frac{B_{2n}}{2}y\right)e^{2q_{10}y}. \tag{73}$$

Only c_1 and c_2 are unknown since the following expressions can be derived:

$$c_3=-\frac{B_{2p}}{4q_{10}}-\frac{1-\frac{\omega}{\alpha}}{4i\alpha g}B_{1p}+\frac{1-\frac{\omega}{\alpha}}{\alpha g}iq_{10}c_1, \tag{74}$$

$$c_4=\frac{B_{2n}}{4q_{10}}-\frac{r-\frac{\omega}{\alpha}}{2i\alpha g}\frac{B_{1n}}{2}+\frac{r-\frac{\omega}{\alpha}}{i\alpha g}q_{10}c_2, \tag{75}$$

where

$$B_{1p}=f_{20v}(+\infty)e^{2qy}, \tag{76}$$

$$B_{2p}=2i\alpha f_{203}(+\infty)e^{2qy}, \tag{77}$$

$$B_{1n}=f_{20v}(-\infty)e^{-2qy}, \tag{78}$$

$$B_{2n}=2i\alpha f_{203}(-\infty)e^{-2qy}. \tag{79}$$

With the foregoing boundary conditions at the two free streams, the coupled differential equations can be integrated from infinity to $y=0$. The two constants c_1 and c_2 are adjusted in an iterative manner until the solutions from the two halves converge at $y=0$: $p_{20}(0^+)=p_{20}(0^-)$, $v_{20}(0^+)=v_{20}(0^-)$. This was achieved using the globally convergent Newton–Raphson iteration method for nonlinear systems of equations.[26]

4. The nonlinear part ϕ_{11}

The nonlinear Eq. (24) contains the unknown Landau constant a_1, which must be obtained in advance before the equations can be solved. The use of an adjoint problem procedure is examined for the purpose of evaluating this constant. The adjoint matrix $\mathbb{M}_{11}^*$ of $\mathbb{M}_{11}$ satisfies the condition

$$\int_{-\infty}^{+\infty}\mathbf{V}_{11}^*\cdot(\mathbb{M}_{11}\mathbf{V}_{11})dy=\int_{-\infty}^{+\infty}\mathbf{V}_{11}\cdot(\mathbb{M}_{11}^*\mathbf{V}_{11}^*)dy, \tag{80}$$

where $\mathbb{M}_{11}$ is defined by Eq. (25) and $\mathbf{V}_{11}^*$ is the adjoint vector of $\mathbf{V}_{11}$. $\mathbf{V}_{11}^*$ satisfies $\mathbb{M}_{11}^*\mathbf{V}_{11}^*=\mathbf{0}$. Therefore,

$$0=\int_{-\infty}^{+\infty}\mathbf{V}_{11}\cdot(\mathbb{M}^*\mathbf{V}_{11}^*)dy=\int_{-\infty}^{+\infty}\mathbf{V}_{11}^*(a_1\mathbf{f}_{10}+\mathbf{f}_{11})dy, \tag{81}$$

so that

$$\int_{-\infty}^{+\infty}\mathbf{V}_{11}^*\cdot a_1\mathbf{f}_{10}\,dy+\int_{-\infty}^{+\infty}\mathbf{V}_{11}^*\cdot\mathbf{f}_{11}\,dy=0 \tag{82}$$

and

$$a_1=-\frac{\int_{-\infty}^{+\infty}\mathbf{V}_{11}^*\cdot\mathbf{f}_{11}\,dy}{\int_{-\infty}^{+\infty}\mathbf{V}_{11}^*\cdot\mathbf{f}_{10}\,dy}. \tag{83}$$

After a little algebra, the adjoint matrix can be written

$$\mathbb{M}_{11}^*=\begin{pmatrix} i(\alpha_3u_{00}-\omega) & 0 & 0 & 0 & 0 & \frac{1}{\gamma M_1^2}T_{00} \\ \rho_{00}i\alpha_3 & \rho_{00}i(\alpha_3u_{00}-\omega) & 0 & 0 & (\gamma-1)i\alpha_3 & 0 \\ -\rho_{00}D & \rho_{00}\frac{du_{00}}{dy} & \rho_{00}i(\alpha_3u_{00}-\omega) & 0 & \rho_{00}\frac{dT_{00}}{dy}-(\gamma-1)D & 0 \\ \rho_{00}i\beta & 0 & 0 & \rho_{00}i(\alpha_3u_{00}-\omega) & (\gamma-1)i\beta & 0 \\ 0 & 0 & 0 & 0 & \rho_{00}i(\alpha_3u_{00}-\omega) & \frac{1}{\gamma M_1^2}\rho_{00} \\ 0 & i\alpha_3 & -D & i\beta & 0 & -1 \end{pmatrix}. \tag{84}$$

The equations $\mathbb{M}_{11}^*\mathbf{V}_{11}^*=\mathbf{0}$ are then reduced to two coupled first-order differential equations for the pressure (p_{11}^*) and y velocity component (v_{11}^*), while the other variables can be expressed in terms of these two variables

$$\frac{dp_{11}^*}{dy}=M_1^2\rho_{00}(\alpha_3u_{00}-\omega)^2v_{11}^*, \tag{85}$$

$$\frac{dv_{11}^*}{dy}=\left[\frac{\alpha_3^2+\beta^2}{M_1^2\rho_{00}(\alpha_3u_{00}-\omega)^2}-1\right]p_{11}^*, \tag{86}$$

$$\rho_{11}^*=\frac{ip_{11}^*}{\gamma M_1^2\rho_{00}(\alpha_3u_{00}-\omega)}, \tag{87}$$

$$u_{11}^*=-\frac{i\alpha_3p_{11}^*}{M_1^2\rho_{00}(\alpha_3u_{00}-\omega)^2}, \tag{88}$$

$$w_{11}^*=-\frac{i\beta p_{11}^*}{M_1^2\rho_{00}(\alpha_3u_{00}-\omega)^2}, \tag{89}$$

$$T_{11}^*=\frac{ip_{11}^*}{\gamma M_1^2(\alpha_3u_{00}-\omega)}. \tag{90}$$

To obtain the boundary conditions at $y\to\pm\infty$, note that the coefficients of v_{11}^* and p_{11}^* are independent of y in those limits and that (85) and (86) can be written as

$$\frac{d^2p_{11}^*}{dy^2}=[\alpha_3^2+\beta^2-M_1^2\rho_{00}(\alpha_3u_{00}-\omega)^2]p_{11}^*=q^{*2}p_{11}^*, \tag{91}$$

$$\frac{d^2v_{11}^*}{dy^2}=[\alpha_3^2+\beta^2-M_1^2\rho_{00}(\alpha_3u_{00}-\omega)^2]v_{11}^*=q^{*2}v_{11}^*, \tag{92}$$

where q^* is defined as

$$q^*=\alpha_3\sqrt{1+\frac{\beta^2}{\alpha_3^2}-M_1^2\rho_{00}\left(u_{00}-\frac{\omega}{\alpha_3}\right)^2}. \tag{93}$$

As $y\to+\infty$, Eqs. (91) and (92) have the general solutions

$$p_{11}^*=c_1e^{-q^*y}, \tag{94}$$

$$v_{11}^*=c_2e^{-q^*y}, \tag{95}$$

where c_1 and c_2 are constants and the terms with positive exponents have been discarded to ensure finite values at the free streams. Inserting these solutions into (85) yields

$$-q^*c_1e^{-q^*y}=M_1^2(\alpha_3-\omega)^2c_2e^{-q^*y}, \tag{96}$$

so that

$$\frac{c_1}{c_2}=-\frac{M_1^2(\alpha_3-\omega)^2}{\alpha_3\sqrt{1+\frac{\beta^2}{\alpha_3^2}-M_1^2\left(1-\frac{\omega}{\alpha_3}\right)^2}}. \tag{97}$$

In the limit $y\to-\infty$, Eqs. (91) and (92) have the general solutions

$$p_{11}^*=c_3e^{q^*y}, \tag{98}$$

$$v_{11}^*=c_4e^{q^*y}, \tag{99}$$

with

$$q^*c_3e^{q^*y}=M_1^2\frac{1}{T_2}(r\alpha_3-\omega)^2c_4e^{q^*y} \tag{100}$$

and

$$\frac{c_3}{c_4}=\frac{M_1^2\frac{1}{T_2}(r\alpha_3-\omega)^2}{\alpha_3\sqrt{1+\frac{\beta^2}{\alpha_3^2}-M_1^2\frac{1}{T_2}\left(r-\frac{\omega}{\alpha_3}\right)^2}}. \tag{101}$$

With these results for p_{11}^* and v_{11}^*, the solutions for ρ_{11}^*, u_{11}^*, w_{11}^*, and T_{11}^* can be obtained as discussed above. More-

over, the Landau constant a_1 is also readily obtained via Eq. (83). Equations (24) can now be simplified and solved,

$$\frac{dv_{11}}{dy}=\frac{\frac{du_{00}}{dy}}{u_{00}-\frac{\omega}{\alpha_3}}v_{11}+\frac{i\alpha_3 g_{11}}{u_{00}-\frac{\omega}{\alpha_3}}p_{11}+f_{11v}, \tag{102}$$

$$\frac{dp_{11}}{dy}=-\rho_{00}i(\alpha_3 u_{00}-\omega)v_{11}+f_{11p}, \tag{103}$$

where

$$g_{11}=T_{00}\left(1+\frac{\beta^2}{\alpha_3^2}\right)-M_1^2\left(u_{00}-\frac{\omega}{\alpha_3}\right)^2, \tag{104}$$

$$f_{11v}=\frac{T_{00}(f_{111}+f'_{111})+(f_{115}+f'_{115})+i(\alpha_3 u_{00}-\omega)f_{116}}{\gamma} - \frac{\alpha_3(f_{112}+f'_{112})+\beta(f_{114}+f'_{114})}{\rho_{00}(\alpha_3 u_{00}-\omega)}, \tag{105}$$

$$f_{11p}=f_{113}+f'_{113}, \tag{106}$$

and

$$f'_{111}=-a_1(\rho_{00}u_{10}+\rho_{10}u_{00}), \tag{107}$$

$$f'_{112}=-a_1\rho_{00}u_{00}u_{10}-a_1p_{10}, \tag{108}$$

$$f'_{113}=-a_1\rho_{00}u_{00}v_{10}, \tag{109}$$

$$f'_{114}=-a_1\rho_{00}u_{00}w_{10}, \tag{110}$$

$$f'_{115}=-a_1\rho_{00}u_{00}T_{10}-(\gamma-1)a_1u_{10}. \tag{111}$$

When y approaches infinity, du_{00}/dy equals zero and the inhomogeneous terms [the right-hand side of Eq. (24)] are complicated and give rise to four possibilities: $\phi_{10}\cdot\psi_{01}$, $\tilde{\phi}_{10}\cdot\psi_{20}$, $\phi_{10}\cdot\psi_{10}\cdot\tilde{\varphi}_{10}$, $a_1\phi_{10}$, all of which have exponential tails but with different decay rates. The analytical formulas for the inhomogeneous terms are then not as easy to derive as those for the other nonlinear components presented in the preceding sections of this paper. A different approach is used for this case.

As $y\to\pm\infty$, Eqs. (102) and (103) become

$$\frac{dv_{11}}{dy}=\frac{g_{11}}{u_{00}-\frac{\omega}{\alpha_3}}p_{11}+f_{11v}, \tag{112}$$

$$\frac{dp_{11}}{dy}=\rho_{00}\alpha_3^2\left(u_{00}-\frac{\omega}{\alpha_3}\right)v_{11}+f_{11p}, \tag{113}$$

or

$$\frac{d^2v_{11}}{dy^2}=q_{11}^2v_{11}+\frac{g_{11}}{u_{00}-\frac{\omega}{\alpha_3}}f_{11p}+f'_{11v}, \tag{114}$$

$$\frac{d^2p_{11}}{dy^2}=q_{11}^2p_{11}+\rho_{00}\alpha_3^2\left(u_{00}-\frac{\omega}{\alpha_3}\right)f_{11v}+f'_{11p}, \tag{115}$$

where

$$q_{11}^2=\rho_{00}\alpha_3^2g_{11} \tag{116}$$

and a prime denotes differentiation with respect to y.

The solution to these equations can be separated into homogeneous and particular parts

$$v_{11}=v_{11h}+v_{11p}, \tag{117}$$

$$p_{11}=p_{11h}+p_{11p}, \tag{118}$$

with

$$v_{11h}=c_1e^{-q_{11}y}+c_2e^{q_{11}y}, \tag{119}$$

$$p_{11h}=c_3e^{-q_{11}y}+c_4e^{q_{11}y}, \tag{120}$$

where

$$c_3=-\frac{q_{11}}{\frac{g}{u_{00}-\frac{\omega}{\alpha_3}}}c_1, \tag{121}$$

$$c_4=\frac{q_{11}}{\frac{g}{u_{00}-\frac{\omega}{\alpha_3}}}c_2. \tag{122}$$

The particular solutions satisfy

$$\frac{d^2v_{11p}}{dy^2}=\frac{g_{11}}{u_{00}-\frac{\omega}{\alpha_3}}p_{11p}+f_{11v}, \tag{123}$$

$$\frac{dp_{11p}}{dy}=\rho_{00}\alpha_3^2\left(u_{00}-\frac{\omega}{\alpha_3}\right)v_{11p}+f_{11p}, \tag{124}$$

which can be solved as

$$v_{11p}=\frac{1}{2q_{11}}\int_{y_0}^{y}[e^{q_{11}(y-t)}-e^{q_{11}(t-y)}]f_{11v}(t)dt, \tag{125}$$

$$p_{11p}=\frac{1}{2q_{11}}\int_{y_0}^{y}[e^{q_{11}(y-t)}-e^{q_{11}(t-y)}]f_{11p}(t)dt, \tag{126}$$

where, for boundedness, we have chosen the negative exponential branch at the fast stream and the positive exponential branch at the slow stream.

The calculation sequence for the whole nonlinear problem is illustrated in Table I, where $\mathbf{V}_{nm}=(\rho_{nm},u_{nm},v_{nm},w_{nm},T_{nm},p_{nm})$. The position (row, column) of each term gives information on the expansion to which it corresponds. For example, $\mathbf{V}_{20}$ is in the row of $A^2e^{2i(\beta z-\omega t)}$ and in the column of $|A|^0$, so $\mathbf{V}_{20}$ comes from the coefficients for $A^2e^{2i(\beta z-\omega t)}$. The terms $\mathbf{V}_{nm}$ are calculated line by line from top to bottom. $\mathbf{V}_{00}$ is the base flow profile, which must be calculated first. The next term is $\mathbf{V}_{10}$, linear eigenfunctions, which must be calculated along with eigenvalue $\alpha=\alpha_R+i\alpha_I$. $\mathbf{V}_{01}$ and $\mathbf{V}_{20}$ are obtained subsequently without requiring further information. Before $\mathbf{V}_{11}$ can be calculated, $a_1=a_{1R}+ia_{1I}$ must be obtained in advance with the knowledge of the known terms.

TABLE I. Illustration of the calculation sequence for the nonlinear problem.

	$\|A\|^0$	$\|A\|^2$	⋯
$A^0 e^{0i(\beta z-\omega t)}$	$\mathbf{V}_{00}$	$\mathbf{V}_{01}$	⋯
$A^1 e^{i(\beta z-\omega t)}$	$\mathbf{V}_{10}$	$\mathbf{V}_{11}$	⋯
$A^2 e^{2i(\beta z-\omega t)}$	$\mathbf{V}_{20}$	⋯	⋯
	⋯	⋯	⋯

IV. RESULTS

The parameters investigated in this study are the convective Mach number M_c, the velocity ratio of the two streams, r, and the density ratio, s. The convective Mach number is defined as $M_c=(U_1^*-U_2^*)/(c_1+c_2)$, where c_1 and c_2 are the nondimensional sound speeds of the two streams. For streams of equal γ (ratio of specific heat at constant pressure and constant volume) and molecular weight, convective Mach number can be related to M_1 as $M_c=[M_1\sqrt{s}(1-r)/(1+\sqrt{s})]$.

The spatial development of amplitude is predicted by Landau equation (11). The present study truncates it to the second term; the two constants α and a_1 associated with the retained terms determine the nature of the amplitude development. The two constants in Eq. (13) play significant roles: $-\alpha_I$ is the growth rate. A negative value of α_I implies a growing disturbance, a positive value represents a decaying disturbance, while zero corresponds to a neutral disturbance. The larger the value of $-\alpha_I$, the faster the disturbance develops. The convective Mach number M_c, velocity ratio r, and density ratio s have strong effects on $-\alpha_{I\max}$, the rate of the fastest growing disturbance. The second constant (a_{1R}) in Landau equation represents the nonlinear effects. The amplitude will converge to an equilibrium value or end in a singularity, depending on whether a_{1R} is negative or positive. Integrating (13) gives

$$|A(x)|^2=\frac{\alpha_I|A|_0^2}{a_{1R}|A|_0^2+(\alpha_I-a_{1R}|A|_0^2)e^{2\alpha_I x}}, \tag{127}$$

where $|A|_0$ is the initial amplitude at the origin ($x=0$). If $a_{1R}>0$, the denominator will approach zero at a finite downstream distance x_s,

$$x_s=-\frac{1}{2\alpha_I}\ln\left(1-\frac{\alpha_I}{a_{1R}|A|_0^2}\right). \tag{128}$$

That is, the amplitude ends in a singularity, signifying the limit of the present procedure. Negative a_{1R} functions as a damping factor which prevents the amplitude from developing indefinitely. The balance between α_I and a_{1R} determines the equilibrium amplitude $|A|^*$. From Eq. (127), $|A|^{*2}\to\alpha_I/a_{1R}$ when $x\to+\infty$. The equilibrium amplitude $|A|^*$ is totally determined by the two constants α_I and a_{1R} in this case. For the linear theory, when $-\alpha_I>0$, the amplitude grows exponentially as $A=e^{-\alpha_I x}$, a potentially unbounded behavior that is terminated by nonlinear effects. The convergence to an equilibrium amplitude under the nonlinear mechanism is shown in Fig. 2. This figure is obtained by integrating Eq. (13) using the calculated value of the eigenvalue α and Landau constant a_1; in the manner discussed earlier in this paper. The parameters α and a_1 determine the final equilibrium value, which is $|A|^*=\sqrt{\alpha_I/a_{1R}}$ and is shown as the solid line in Fig. 2. The dashed line in Fig. 2 represents the solution of Eq. (13) when the initial amplitude $|A|_1$ is such that $|A|_1\gg|A|^*$, whereas the dashed–dotted line is for $|A|_1\ll|A|^*$. Obviously, the latter situation takes longer to reach equilibrium ($x\approx60$) compared to the case with higher initial amplitude ($x\approx20$). When $|A|$ is large, the second term, which is the fourth power of the amplitude, is more significant. Consequently, the drop to the equilibrium amplitude $|A|^*$ is very rapid. When the initial amplitude $|A|$ is small (and less than unity), the first term is dominant, leading to results that are similar to those of the linear theory. Further growth in $|A|$ causes increasing importance of nonlinear effects. The present studies focus on the case with small initial amplitude.

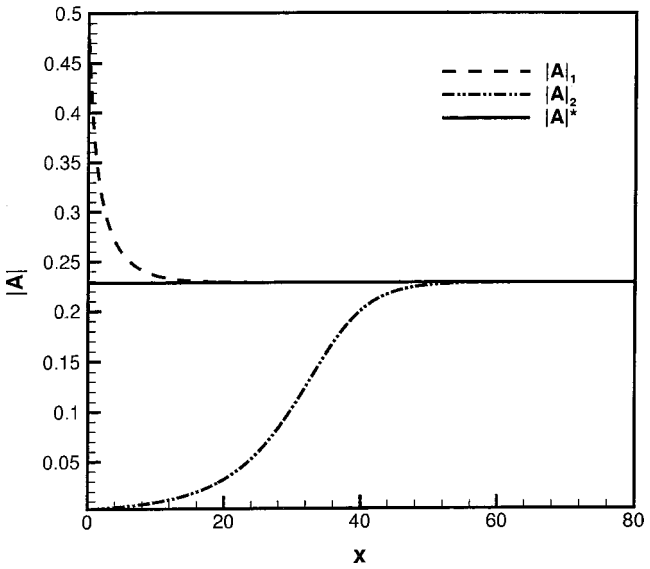

FIG. 2. Convergence to the equilibrium amplitude $|A|^*$.

Figures 3(a)–3(d) illustrate the pressure solution as a function of the downstream distance. The linear results in Fig. 3(a) show essentially zero values up until approximately $x\approx12.5$, beyond which an oscillatory pattern evolves. The amplitude of the oscillation grows from zero to approximately $|p|_{10}\approx0.7E-05$ at $x\approx60$, after which a limit cycle is maintained. Note that the point $x\approx60$ coincides with the location where the equilibrium amplitude $|A|^*$ is established (Fig. 2). Therefore, the downstream growth of $|A|$ is directly correlated with the growth in pressure eigenfunction. Surprisingly, the nonlinear eigenfunction p_{01} does not show an oscillatory pattern but rather a hyperbolic tangent profile. The p_{11} component of the eigenfunction shows a similar trend to p_{10}, although its development starts at a much later location ($x\approx35$) and its amplitude is an order of magnitude weaker. Note that both disturbances show a wavelength λ, of approximately 7.5. The nonlinear eigenfunction p_{20} has a relatively strong amplitude ($0.7E-03$). We also observe wave number doubling ($\lambda\approx3.75$) relative to the component p_{01} or p_{11}. This eigenfunction also exhibits a limit cycle shortly after the equilibrium amplitude is established.

The distributions along y of the linear eigenfunctions for

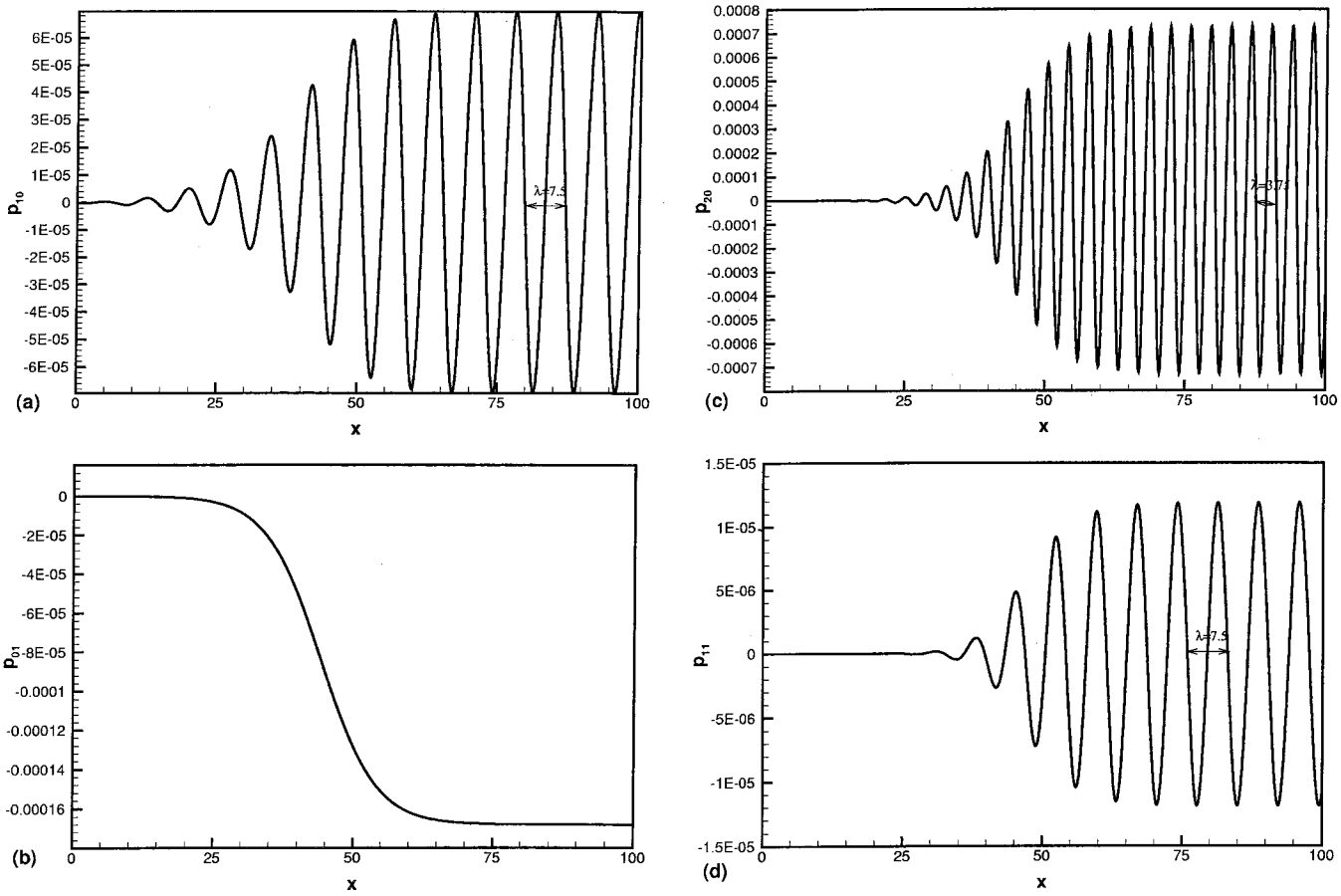

FIG. 3. The perturbation waves: (a) p_{10}, (b) p_{01}, (c) p_{20}, (d) p_{11}. The parameters are $M_c=0.25$, $r=0$, and $s=1$.

u, v, ρ, T, and p are shown in Figs. 4(a)–4(e). These plots show the real component (ϕ_r), the imaginary component (ϕ_i), and the magnitude ($\sqrt{\phi_r^2+\phi_i^2}$). For u_{10}, the imaginary component is dominant and is roughly symmetric about $y=0$. The real component has the greater contribution around $y=-1$ and $y=0.5$. For v_{10}, the real component is dominant and symmetric about $y=0$. The imaginary component has the larger contribution around $y=\pm 0.5$, with essentially zero contribution at $y=0$. This component is also antisymmetric about $y=0$.

The distribution of ρ_{10} and T_{10} are strongly but negatively correlated for both the real and imaginary components, leading to magnitudes of ρ_{10} and T_{10} that have similar y profile [Figs. 4(c) and 4(d)]. Unlike the distributions of u_{10} and v_{10}, which have longer tails ($-5\leqslant y\leqslant 5$), the density and temperature eigenfunctions are mostly restricted to $|y|\leqslant 2$. The pressure contributions come essentially from the real component of the eigenfunction, as the imaginary component is essentially zero for all y. The pressure effects are found in $|y|\leqslant 5$ [Fig. 4(f)].

Concerning the validity of the linear results in Figs. 4(a)–4(f), it is important to realize that they were obtained (''post-processed'') from the same analysis that have shown good agreement with the results of DRM, more details of which are provided below.

Figures 5–7 illustrate the effects of compressibility (convective Mach number), velocity ratio, r, and density ratio, s, on the maximum linear growth rate ($-\alpha_{I\,\max}$), the nonlinear growth coefficient a_{1R}, and the equilibrium amplitude $|A|^*$. The maximum growth rate results for the linear case are shown in Figs. 5(a), 6(a), and 7(a) as a function of M_c, r, and s, respectively. In these figures, the linear results from the present studies are also compared with those of DRM, who used a different method of analysis and restricted their analysis to the linear problem. In general, the agreement between their results and the present results is very good, thereby giving some validity to the procedure used in the present work for both the linear and nonlinear problems.

Figure 5(a) shows a parabolic decay in the maximum growth rate as the convective Mach number M_c increases, in accordance with the well known results for the linear problem that compressibility has a stabilizing effect on the growth rate. Beyond $M_c\approx 0.8$, the decay is weaker and assumes an approximately linear profile with M_c. The nonlinear growth rate a_{1R} shows an opposite behavior to the maximum (linear) growth rate [Fig. 5(b)]. That is, it is characterized by an initial parabolic growth with M_c, until $M_c\approx 0.8$, after which the growth is significantly reduced and a_{1R} becomes essentially independent of M_c, with a saturation value of $a_{1R}\approx 2.6$. From these results, therefore, we can observe a negative correlation between the maximum (linear)

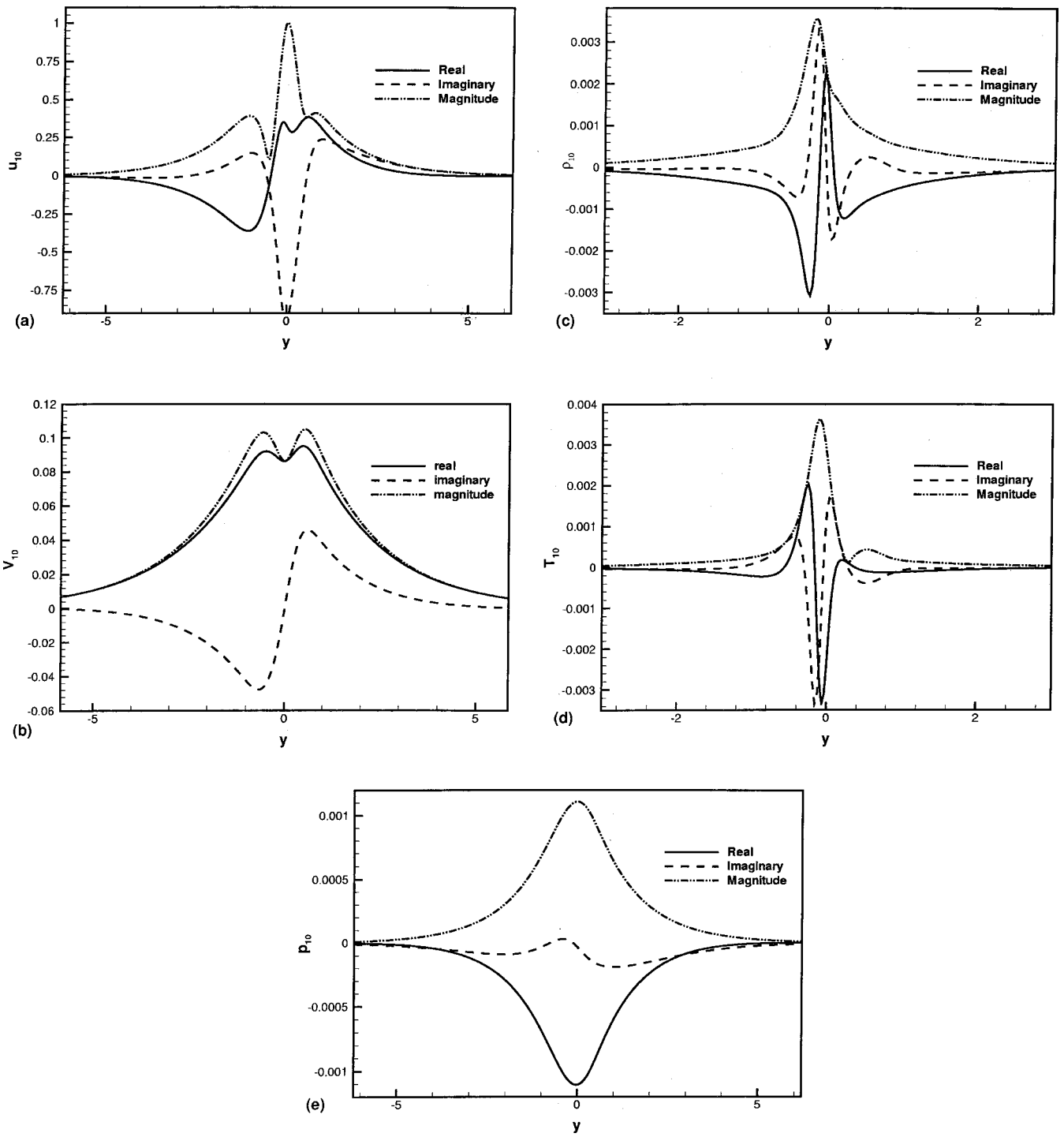

FIG. 4. The linear eigenfunctions: (a) u_{10}, (b) v_{10}, (c) ρ_{10}, (d) T_{10}, (e) p_{10}. The parameters are $M_c=0.6$, $r=0$, and $s=1$.

growth rate of the linear component and the nonlinear coefficient a_{1R}. Note that a_{1R} becomes positive at $M_c=0.5$ and saturates at $M_c=0.8$. From the foregoing, it is apparent that the present study gives a perfect agreement with the results of DRM for the maximum growth rate for M_c up to 2.0. However, there seems to be some kind of degeneracy around $M_c=0.5$. This is evident in Fig. 5(c), where the equilibrium amplitude shows a steep increase with M_c as M_c approaches 0.5. When $M_c>0.5$, the distance x_s required for the perturbation to end in a singularity is shortened, as per Eq. (128). That is, the higher the convective Mach number, the shorter the perturbation waves travel. In the asymptotic limit $M_c \to \infty$, this distance approaches zero. In this limit, a multiple scale analysis, such as in Balsa and Goldstein[27] might be more appropriate than the present Landau procedure. Furthermore, note that the unboundedness of the nonlinear amplitude might not be observed in a physical system since, unlike the inviscid model, viscosity is present and will provide the necessary dissipation to prevent this behavior.

The effect of r on the maximum growth rate is shown in Fig. 6(a), where agreement is evident between the DRM re-

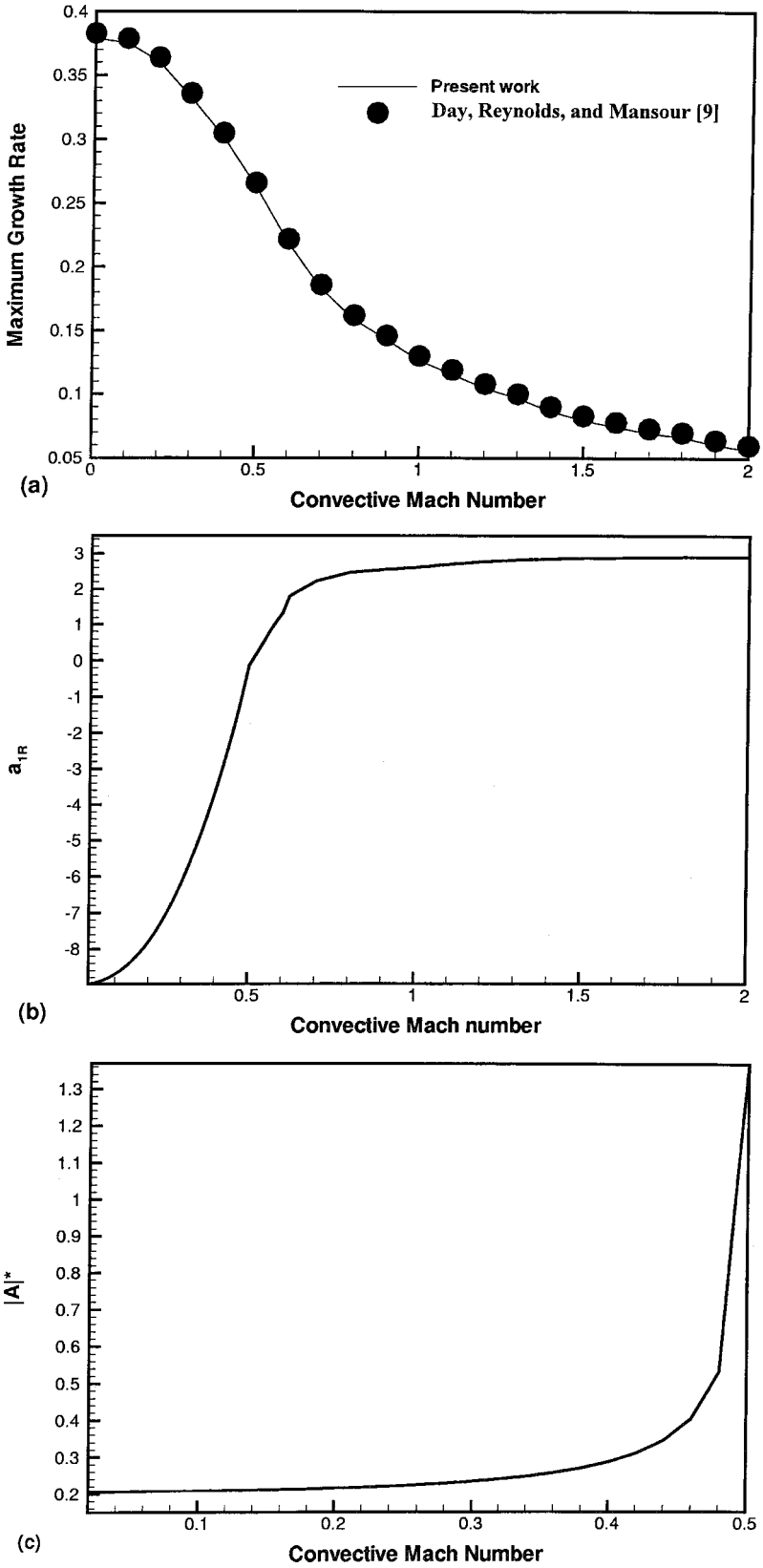

FIG. 5. The effects of compressibility on (a) maximum growth rate ($-\alpha_I$), (b) a_{1R}, (c) the equilibrium amplitude $|A|^*$. The parameters are $r=0$ and $s=1$.

sults and the present study. The exponential growth rate at smaller r values is replaced by a fairly linear decay at larger r values ($r\approx 0.24$). Unlike the linear results which show a monotonic behavior, the nonlinear parameter a_{1R} shows a nonmonotonic dependence on r, with a local maximum occurring at $r\approx 0.24$, which coincides with the beginning of the slow decay in the maximum growth rate. a_{1R} has an average value of approximately -11 until $r\approx 0.73$ [Fig. 6(b)]. The equilibrium amplitude shows a fairly monotonic decay with r [Fig. 6(c)], starting off at a gradient of ≈ -0.25 for $x \leqslant 0.12$, slowing down to a gradient of -0.15 for $0.12 \leqslant x \leqslant 0.73$ and leveling off to a constant value thereafter.

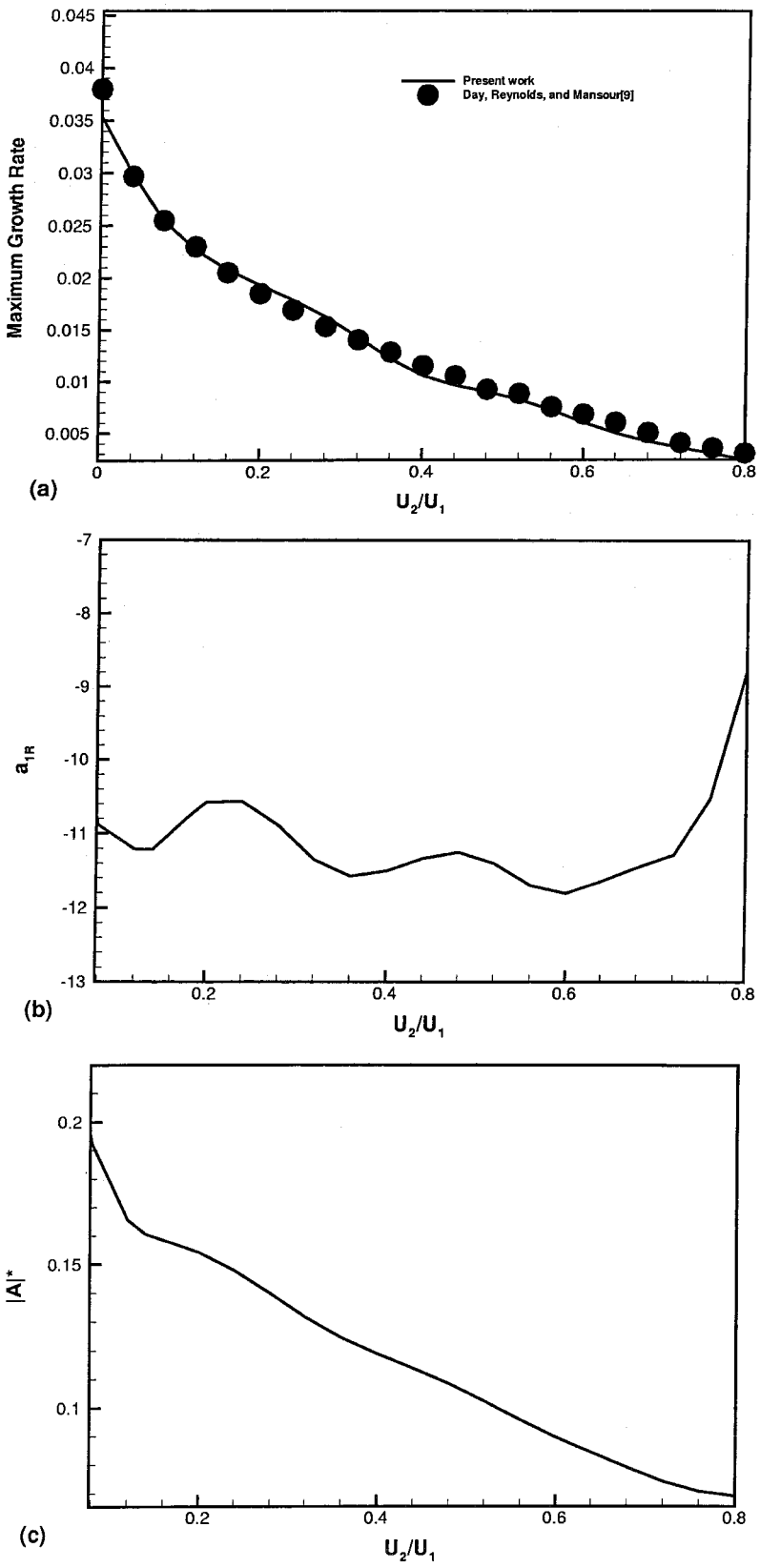

FIG. 6. The effects of velocity ratio $r \equiv U_2/U_1$ on (a) maximum growth rate $(-\alpha_I)$, (b) a_{1R}, (c) the equilibrium amplitude $|A|^*$. The parameters are $M_c = 2.75$ and $s = 1$.

The dependence of the maximum growth rate on the density ratio s is a perfect straight line, with a gradient of $+0.2$ [Fig. 7(a)]. This result is obtained in both DRM and the present studies. The nonlinear coefficient a_{1R} decreases with s for $s < 3.6$. The decay is generally nonlinear (nonmonotonic), although it can be approximated between $0 \leqslant s \leqslant 3.6$ by a straight line with a gradient of -4.2. For $s > 3.6$, a_{1R} increases with a steep gradient of $+25.0$. The equilibrium amplitude drops rapidly with density ratio at small values of the density ratio ($s < 0.6$). Beyond this point, i.e., $0.6 \leqslant s \leqslant 4.0$,

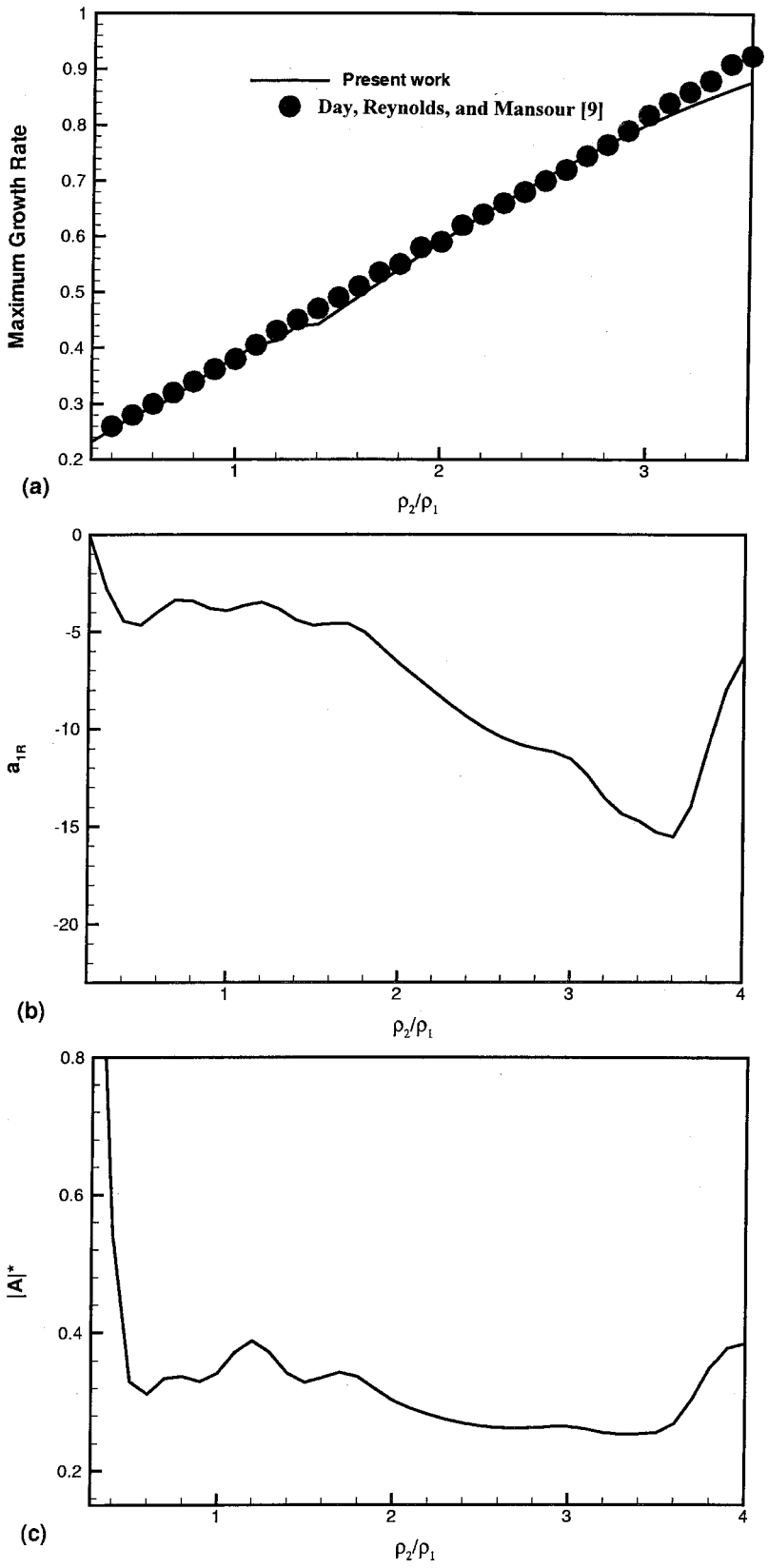

FIG. 7. The effects of density ratio $s \equiv \rho_2/\rho_1$ on (a) maximum growth rate $(-\alpha_I)$, (b) a_{1R}, (c) the equilibrium amplitude $|A|^*$. The parameters are $M_c = 0$ and $r = 0$.

the equilibrium amplitude oscillates about $|A|^* \approx 0.34$.

Referring to Fig. 4, it can be seen that the linear eigenfunctions (u_{10}, v_{10}, ρ_{10}, T_{10}, and p_{10}) decay exponentially as the two boundaries $y = \pm\infty$ are approached. As mentioned earlier, this is a condition that limits the linear analysis to subsonic disturbances and therefore to region one in the phase speed-Mach number diagram of Grosch and Jackson.[8] The nonlinear eigenfunctions (u_{01}, v_{01}, ρ_{01}, T_{01}, and p_{01}) show a different behavior at the boundaries. For the fast stream, the nature of the boundary solutions depend on the

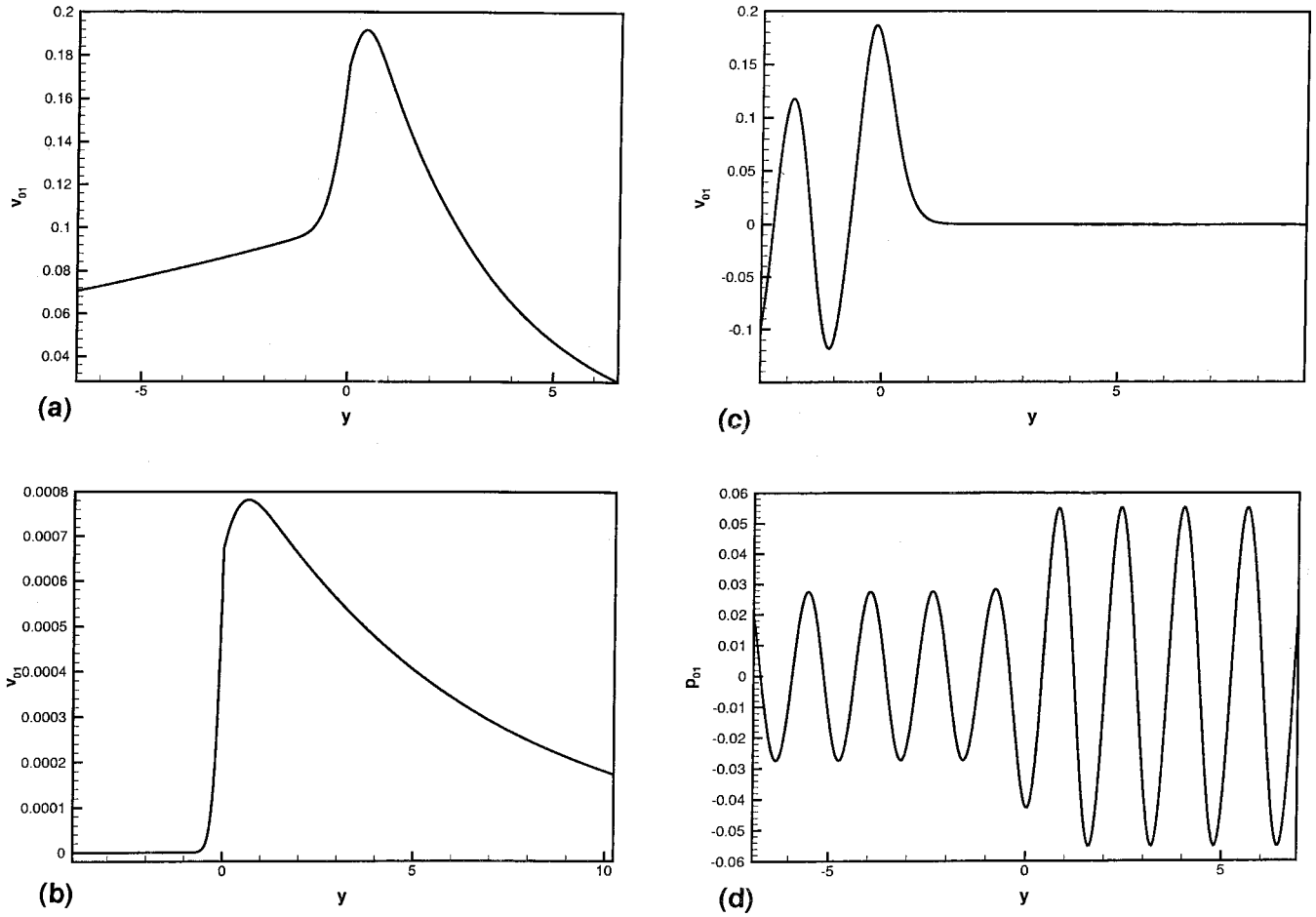

FIG. 8. The dependence of the boundary solutions on M_1 (fast stream) and $M_1^2sr^2$ (slow stream). The conditions at the boundaries are (a) v_{01}, $M_1=1.25$, $M_1^2sr^2=1.25$; (b) v_{01}, $M_1=1.25$, $M_1^2sr^2=1.0$; (c) v_{01}, $M_1=1.0$, $M_1^2sr^2=0.6$; (d) p_{01}, $M_1=0.6$, $M_1^2sr^2=0.6$.

sign of M_1^2-1. For $M_1^2>1$, the disturbances decay; for $M_1^2=1$, the disturbances approach a constant value, whereas for $M_1^2<1$, they oscillate in y. Since $M_1<1$ for the latter case, the net velocity away from the boundary, $\pm u+c$, is positive, where u is the fluid velocity normal to the boundary. Therefore, the oscillations represent outgoing waves. Figures 8(a) and 8(b) show a decaying disturbance at $+\infty$ where $M_1=1.25>1$. On the other hand, Fig. 8(c) shows a fairly constant behavior ($M_1=1$). A wave solution at this boundary is evident in Fig. 8(d), where $M_1=0.6$. According to the theory in Sec. III B 2, the wavelength $\lambda_{+\infty}$ of the oscillations is $\lambda_{+\infty}=\pi/|\alpha_I|\sqrt{1-M_1^2}$, which approaches infinity as $M_1\rightarrow 1$, consistent with the $M_1=1$ limit of a constant signal at the boundary.

For the slow stream, the occurrence of decaying, constant, and outgoing wave solutions depend on the sign of the discriminant $M_1^2sr^2-1$, which has to be greater, equal, or less than zero for the respective types of boundary solutions. This behavior can be observed in Figs. 8(a)–8(d). In this case, the wavelength of the oscillations is $\lambda_{-\infty}=\pi/|\alpha_I|\sqrt{1-M_1^2sr^2}$. Note that, unlike the boundary solutions at the fast stream, which depend only on the values of M_1, the condition $r=0$ always leads to solutions which oscillate at $y\rightarrow-\infty$ for any M_1.

To advance an explanation for the apparently strange behavior described above, it should be noted that subsonic flows are in general more prone to oscillations (Ghosh and Matthaeus[31] and Ladeinde *et al.*[32]), compared to incompressible or sonic/supersonic flows. These oscillations are nonlinear, Euler effects, which explains their suppression in the linear problem. As the effective Mach number increases toward the sonic and supersonic limits, the manifestation of the nonlinear solutions is usually in terms of exponential decay (growth) or constants, as wave steepening becomes important. A discontinuity in the solutions, caused by shock waves, is therefore a possibility, even though we have not explicitly identified this in the present work. Furthermore, it is not inconceivable that the unboundedness alluded to earlier in this paper for increasing Mach number is a manifestation of incipient discontinuity brought about by wave steepening. None of the existing nonlinear stability methods,[6,23–25] including the present one can analyze the discontinuous phenomena. In this case, the method of characteristics might perform better, although we cannot be definitive about this issue. Finally, note that in the foregoing, the quantity $\sqrt{M_1^2sr^2}$ is the effective Mach number of the slow stream, leading to an effective sonic limit of $\sqrt{M_1^2sr^2}=1$.

V. CONCLUDING REMARKS

The weakly nonlinear behavior of compressible mixing layers is investigated analytically in this paper, using the Landau's procedure. The nonlinear stability to three-dimensional perturbation waves is analyzed by expanding the perturbations into amplitude-dependent harmonic waves and truncating the Landau equation to the second term. The basic procedure in this paper is similar to that in Liu[22] for compressible laminar wakes. However, Liu did not present any results for his analysis. The present paper has many interesting results, including the effects of velocity ratio, density ratio, and convective Mach number on the linear growth rate, the nonlinear contribution to perturbation growth, and the magnitude and distribution of the equilibrium amplitude, $|A|^*$. The linear results from the present analysis compare very well with those reported by Day, Reynolds, and Mansour,[9] who employed a different procedure and limited their analysis to the linear regime. We have observed in the present studies that, although the linear analysis is restricted to exponentially decaying linear solutions at the boundaries, nonlinear effects could introduce constant, decaying, or outgoing wave solutions at the boundaries, depending on the velocity and density ratios and the Mach number of the fast stream.

ACKNOWLEDGMENTS

This work was supported by the National Science Foundation under CTS-9626413. The contribution of Professor Edward E. O'Brien and Dr. Xiaodan Cai to an earlier version of this paper is gratefully acknowledged, as is a similar contribution by Professor James Glimm.

APPENDIX: SOURCE TERMS

The inhomogeneous terms in the ODEs for the eigenfunctions are defined in this appendix.

(a) $\mathbf{f}_{01}$: The inhomogeneous term $\mathbf{f}_{01}$ in Eq. (20) is defined. It is composed of six elements:

$$\mathbf{f}_{01}=(f_{011},f_{012},f_{013},f_{014},f_{015},f_{016})^T, \tag{A1}$$

where

$$f_{011}=-2\,\mathrm{Re}\left[\tilde{p}_{10}\left(i(\alpha u_{10}+\beta w_{10})+\frac{dv_{10}}{dy}\right)\right]-2\,\mathrm{Re}\left[\rho_{10}i(\alpha\tilde{u}_{10}+\beta\tilde{w}_{10})+\tilde{v}_{10}\frac{d\rho_{10}}{dy}\right], \tag{A2}$$

$$f_{012}=-2\,\mathrm{Re}\left[\rho_{00}\left(i(\alpha\tilde{u}_{10}+\beta\tilde{w}_{10})u_{10}+\tilde{v}_{10}\frac{du_{10}}{dy}\right)\right]-2\,\mathrm{Re}\left[\tilde{p}_{10}\left(i(\alpha u_{00}-\omega)u_{10}+v_{10}\frac{du_{00}}{dy}\right)\right], \tag{A3}$$

$$f_{013}=-2\,\mathrm{Re}\left[\rho_{00}\left(i(\alpha\tilde{u}_{10}+\beta\tilde{w}_{10})v_{10}+\tilde{v}_{10}\frac{dv_{10}}{dy}\right)\right]-2\,\mathrm{Re}[\tilde{p}_{10}i(\alpha u_{00}-\omega)v_{10}], \tag{A4}$$

$$f_{014}=-2\,\mathrm{Re}[\tilde{p}_{10}i(\alpha u_{00}-\omega)w_{10}]-2\,\mathrm{Re}\left[\rho_{00}\left(i(\alpha\tilde{u}_{10}+\beta\tilde{w}_{10})w_{10}+\tilde{v}_{10}\frac{dw_{10}}{dy}\right)\right], \tag{A5}$$

$$f_{015}=2\,\mathrm{Re}[\rho_{10}i(\alpha u_{00}-\omega)\tilde{T}_{10}]-2\,\mathrm{Re}\left[\rho_{00}\left(i(\alpha\tilde{u}_{10}+\beta\tilde{w}_{10})T_{10}+\tilde{v}_{10}\frac{dT_{10}}{dy}\right)\right]-2\,\mathrm{Re}\left(\rho_{10}\tilde{v}_{10}\frac{dT_{00}}{dy}\right)-2\,\mathrm{Re}\left[\gamma M_1^2(\gamma-1)\tilde{p}_{10}\left(i(\alpha u_{10}+\beta w_{10})+\frac{dv_{10}}{dy}\right)\right], \tag{A6}$$

$$f_{016}=-\frac{2}{\gamma M_1^2}\mathrm{Re}(\rho_{10}\tilde{T}_{10}). \tag{A7}$$

(b) $\mathbf{f}_{20}$: The inhomogeneous term $\mathbf{f}_{20}$ in Eq. (22) is defined. It is composed of six elements:

$$\mathbf{f}_{20}=(f_{201},f_{202},f_{203},f_{204},f_{205},f_{206})^T, \tag{A8}$$

where

$$f_{201}=-\rho_{10}2i(\alpha u_{10}+\beta w_{10})-\frac{d(\rho_{10}v_{10})}{dy}, \tag{A9}$$

$$f_{202}=-\rho_{00}\left[i(\alpha u_{10}+\beta w_{10})u_{10}+v_{10}\frac{du_{10}}{dy}\right]-\rho_{10}\left[i(\alpha u_{00}-\omega)u_{10}+v_{10}\frac{du_{00}}{dy}\right], \tag{A10}$$

$$f_{203}=-\rho_{00}\left[i(\alpha u_{10}+\beta w_{10})v_{10}+v_{10}\frac{dv_{10}}{dy}\right]-\rho_{10}i(\alpha u_{00}-\omega)v_{10}, \tag{A11}$$

$$f_{204}=-\rho_{00}\left[i(\alpha u_{10}+\beta w_{10})w_{10}+v_{10}\frac{dw_{10}}{dy}\right]-\rho_{10}i(\alpha u_{00}-\omega)w_{10}, \tag{A12}$$

$$f_{205}=-\rho_{10}i(\alpha u_{00}-\omega)T_{10}-\rho_{10}v_{10}\frac{dT_{00}}{dy}-\rho_{00}\left[i(\alpha u_{10}+\beta w_{10})T_{10}+v_{10}\frac{dT_{10}}{dy}\right]-\gamma M_1^2(\gamma-1)p_{10}\left[i(\alpha u_{10}+\beta w_{10})+\frac{dv_{10}}{dy}\right], \tag{A13}$$

$$f_{206}=-\frac{1}{\gamma M_1^2}\rho_{10}T_{10}. \tag{A14}$$

(c) $\mathbf{f}_{10}$ and $\mathbf{f}_{11}$: The inhomogeneous terms $\mathbf{f}_{10}$ and $\mathbf{f}_{11}$ in Eq. (24). The elements of each are

$$\mathbf{f}_{10}=-\begin{pmatrix}\rho_{00}u_{10}+\rho_{10}u_{00}\\ \rho_{00}u_{00}u_{10}+p_{10}\\ \rho_{00}u_{00}v_{10}\\ \rho_{00}u_{00}w_{10}\\ \rho_{00}u_{00}T_{10}+(\gamma-1)u_{10}\\ 0\end{pmatrix}, \tag{A15}$$

$$\mathbf{f}_{11}=(f_{111},f_{112},f_{113},f_{114},f_{115},f_{116})^T, \tag{A16}$$

where

$$\begin{aligned}f_{111}=&-\rho_{10}\left(i(\alpha u_{01}+\beta w_{01})+\frac{dv_{01}}{dy}\right)-\tilde{\rho}_{10}\left(2i(\alpha u_{20}+\beta w_{20})+\frac{dv_{20}}{dy}\right)-\rho_{01}\left(i(\alpha u_{10}+\beta w_{10})+\frac{dv_{10}}{dy}\right)\\&+\tilde{\rho}_{10}i(\tilde{\alpha}u_{20}+\beta w_{20})-\rho_{20}2i(\alpha\tilde{u}_{10}+\beta\tilde{w}_{10})-\rho_{20}\left(-i(\tilde{\alpha}\tilde{u}_{10}+\beta\tilde{w}_{10})+\frac{d\tilde{v}_{10}}{dy}\right)\\&+2\alpha_I\rho_{10}u_{01}+2\alpha_I\rho_{01}u_{10}-v_{10}\frac{d\rho_{01}}{dy}-v_{01}\frac{d\rho_{10}}{dy}-\tilde{v}_{10}\frac{d\rho_{20}}{dy}-v_{20}\frac{d\tilde{\rho}_{10}}{dy},\end{aligned} \tag{A17}$$

$$\begin{aligned}f_{112}=&-\rho_{01}i(\alpha u_{00}-\omega)u_{10}-\rho_{00}\left[i(\alpha u_{01}+\beta w_{01})u_{10}+v_{01}\frac{du_{10}}{dy}\right]-\rho_{00}\left[2i(\alpha\tilde{u}_{10}+\beta\tilde{w}_{10})u_{20}+\tilde{v}_{10}\frac{du_{20}}{dy}\right]\\&-\rho_{00}\left[-i(\tilde{\alpha}u_{20}+\beta w_{20})\tilde{u}_{10}+v_{20}\frac{d\tilde{u}_{10}}{dy}\right]-\rho_{10}\left[-i(\tilde{\alpha}u_{10}+\beta w_{10})\tilde{u}_{10}+v_{10}\frac{d\tilde{u}_{10}}{dy}\right]\\&-\rho_{10}\left[i(\alpha\tilde{u}_{10}+\beta\tilde{w}_{10})u_{10}+\tilde{v}_{10}\frac{du_{10}}{dy}\right]-\tilde{\rho}_{10}2i(\alpha_0u_{00}-\omega)u_{20}+\rho_{20}i(\tilde{\alpha}u_{00}-\omega)\tilde{u}_{10}\\&-\tilde{\rho}_{10}\left[i(\alpha u_{10}+\beta w_{10})u_{10}+v_{10}\frac{du_{10}}{dy}\right]+2\alpha_I(\rho_{00}u_{10}u_{01}+\rho_{10}u_{00}u_{01})\\&-\rho_{00}v_{10}\frac{du_{01}}{dy}-\rho_{01}v_{10}\frac{du_{00}}{dy}-\rho_{10}v_{01}\frac{du_{00}}{dy}-\tilde{\rho}_{10}v_{20}\frac{du_{00}}{dy}-\rho_{20}\tilde{v}_{10}\frac{du_{00}}{dy},\end{aligned} \tag{A18}$$

$$\begin{aligned}f_{113}=&-\rho_{01}i(\alpha u_{00}-\omega)v_{10}-\tilde{\rho}_{10}2i(\alpha u_{00}-\omega)v_{20}-\rho_{00}\left[i(\alpha u_{01}+\beta w_{01})v_{10}+v_{01}\frac{dv_{10}}{dy}\right]\\&-\rho_{00}\left[2i(\alpha\tilde{u}_{10}+\beta\tilde{w}_{10})v_{20}+\tilde{v}_{10}\frac{dv_{20}}{dy}\right]-\rho_{00}\left[-i(\tilde{\alpha}u_{20}+\beta w_{20})\tilde{v}_{10}+v_{20}\frac{d\tilde{v}_{10}}{dy}\right]\\&-\rho_{10}\left[-i(\tilde{\alpha}u_{10}+\beta w_{10})\tilde{v}_{10}+v_{10}\frac{d\tilde{v}_{10}}{dy}\right]-\rho_{10}\left[i(\alpha\tilde{u}_{10}+\beta\tilde{w}_{10})v_{10}+\tilde{v}_{10}\frac{dv_{10}}{dy}\right]\\&-\tilde{\rho}_{10}\left[i(\alpha u_{10}+\beta w_{10})v_{10}+v_{10}\frac{dv_{10}}{dy}\right]+\rho_{20}i(\tilde{\alpha}u_{00}-\omega)\tilde{v}_{10}-\rho_{00}v_{10}\frac{dv_{01}}{dy}\\&+2\alpha_I(\rho_{00}u_{10}v_{01}+\rho_{10}u_{00}v_{01}),\end{aligned} \tag{A19}$$

$$\begin{aligned}f_{114}=&-\rho_{01}i(\alpha u_{00}-\omega)w_{10}-\tilde{\rho}_{10}2i(\alpha u_{00}-\omega)w_{20}+\rho_{20}i(\tilde{\alpha}u_{00}-\omega)\tilde{w}_{10}\\&-\rho_{00}\left[i(\alpha u_{01}+\beta w_{01})w_{10}+v_{01}\frac{dw_{10}}{dy}\right]-\rho_{00}v_{10}\frac{dw_{01}}{dy}-\rho_{00}\left[2i(\alpha\tilde{u}_{10}+\beta\tilde{w}_{10})w_{20}+\tilde{v}_{10}\frac{dw_{20}}{dy}\right]\\&-\rho_{00}\left[-i(\tilde{\alpha}u_{20}+\beta w_{20})\tilde{w}_{10}+v_{20}\frac{d\tilde{w}_{10}}{dy}\right]-\rho_{10}\left[-i(\tilde{\alpha}u_{10}+\beta w_{10})\tilde{w}_{10}+v_{10}\frac{d\tilde{w}_{10}}{dy}\right]\\&-\rho_{10}\left[i(\alpha\tilde{u}_{10}+\beta\tilde{w}_{10})w_{10}+\tilde{v}_{10}\frac{dw_{10}}{dy}\right]-\tilde{\rho}_{10}\left[i(\alpha u_{10}+\beta w_{10})w_{10}+v_{10}\frac{dw_{10}}{dy}\right]\\&+2\alpha_I(\rho_{00}u_{10}w_{01}+\rho_{10}u_{00}w_{01}),\end{aligned} \tag{A20}$$

$$f_{115}=-\rho_{01}i(\alpha u_{00}-\omega)T_{10}-\tilde{\rho}_{10}2i(\alpha u_{00}-\omega)T_{20}+\rho_{20}i(\tilde{\alpha}u_{00}-\omega)\tilde{T}_{10}-\rho_{00}\left[i(\alpha u_{01}+\beta w_{01})T_{10}+v_{01}\frac{dT_{10}}{dy}\right]$$
$$-\rho_{00}\left[2i(\alpha\tilde{u}_{10}+\beta\tilde{w}_{10})T_{20}+\tilde{v}_{10}\frac{dT_{20}}{dy}\right]-\rho_{00}\left[-i(\tilde{\alpha}u_{20}+\beta w_{20})\tilde{T}_{10}+v_{20}\frac{d\tilde{T}_{10}}{dy}\right]$$
$$-\rho_{10}\left[-i(\tilde{\alpha}u_{10}+\beta w_{10})\tilde{T}_{10}+v_{10}\frac{d\tilde{T}_{10}}{dy}\right]-\rho_{10}\left[i(\alpha\tilde{u}_{10}+\beta\tilde{w}_{10})T_{10}+\tilde{v}_{10}\frac{dT_{10}}{dy}\right]$$
$$-\tilde{\rho}_{10}\left[i(\alpha u_{10}+\beta w_{10})T_{10}+v_{10}\frac{dT_{10}}{dy}\right]+2\alpha_I(\rho_{00}u_{10}T_{01}+\rho_{10}u_{00}T_{01})-\rho_{00}v_{10}\frac{dT_{01}}{dy}$$
$$-\rho_{01}v_{10}\frac{dT_{00}}{dy}-\rho_{10}v_{01}\frac{dT_{00}}{dy}-\tilde{\rho}_{10}v_{20}\frac{dT_{00}}{dy}-\rho_{20}\tilde{v}_{10}\frac{dT_{00}}{dy}-\gamma M_1^2(\gamma-1)p_{01}\left[i(\alpha u_{10}+\beta w_{10})+\frac{dv_{10}}{dy}\right]$$
$$-\gamma M_1^2(\gamma-1)p_{10}\left[-2\alpha_I u_{01}+\frac{dv_{01}}{dy}\right]-\gamma M_1^2(\gamma-1)\tilde{p}_{10}\left[2i(\alpha u_{20}+\beta w_{20})+\frac{dv_{20}}{dy}\right]$$
$$-\gamma M_1^2(\gamma-1)p_{20}\left[-i(\tilde{\alpha}\tilde{u}_{10}+\beta\tilde{w}_{10})+\frac{d\tilde{v}_{10}}{dy}\right], \tag{A21}$$

$$f_{116}=-\frac{1}{\gamma M_1^2}(\rho_{01}T_{10}+\rho_{10}T_{01}+\tilde{\rho}_{10}T_{20}+\rho_{20}\tilde{T}_{10}). \tag{A22}$$

[1] A. Michalke, "On the inviscid instability of the hyperbolic-tangent velocity profile," J. Fluid Mech. **19**, 543 (1964).
[2] A. Michalke, "Vortex formation in a free boundary layer according to stability theory," J. Fluid Mech. **22**, 371 (1965).
[3] A. Michalke, "On spatially growing disturbance in an inviscid shear layer," J. Fluid Mech. **23**, 521 (1965).
[4] G. Brown and A. Roshko, "On the density effects and large structure in turbulence mixing layers," J. Fluid Mech. **64**, 775 (1974).
[5] M. Lesson, J. A. Fox, and H. M. Zien, "On the inviscid stability of the laminar mixing of two parallel streams of a compressible fluid," J. Fluid Mech. **23**, 355 (1965).
[6] M. E. Goldstein and S. J. Leib, "Nonlinear evolution of oblique waves on compressible shear layers," J. Fluid Mech. **207**, 73 (1989).
[7] C. E. Grosch and T. L. Jackson, "Inviscid spatial stability of a three-dimensional, compressible mixing layer," J. Fluid Mech. **231**, 35 (1991).
[8] T. L. Jackson and C. E. Grosch, "Inviscid spatial stability of a compressible mixing layer," J. Fluid Mech. **208**, 609 (1989).
[9] M. J. Day, W. C. Reynolds, and N. N. Mansour, "The structure of the compressible reacting mixing layer: Insights from linear stability analysis," Phys. Fluids **10**, 993 (1998).
[10] O. H. Planché and W. C. Reynolds, "Heat release effects on mixing in supersonic reacting free shear-layers," AIAA Paper AIAA-92-0092 (1992).
[11] S. A. Ragab and J. L. Wu, "Linear instability in two-dimensional compressible mixing layers," Phys. Fluids A **1**, 957 (1989).
[12] H. Schade, "Contribution to the nonlinear stability theory of inviscid shear layers," Phys. Fluids **7**, 623 (1964).
[13] A. W. Vreman, N. D. Sandham, and K. H. Luo, "Compressible mixing layer growth rate and turbulence characteristics," J. Fluid Mech. **320**, 235 (1996).
[14] D. Papamoschou and A. Roshko, "The compressible turbulent shear layer: An experimental study," J. Fluid Mech. **197**, 453 (1988).
[15] F. Ladeinde and K. E. Torrance, "Convection in rotating, horizontal cylinders with radial and normal gravity forces," J. Fluid Mech. **228**, 361 (1991).
[16] N. D. Sandham and W. C. Reynolds, "Compressible mixing layer: Linear theory and direct simulation," AIAA J. **28**, 618 (1990).
[17] J. T. Stuart, "On the non-linear mechanics of hydrodynamic stability," J. Fluid Mech. **4**, 1 (1958).
[18] E. Palm, "On the tendency towards hexagonal cells in steady convection," J. Fluid Mech. **8**, 183 (1960).
[19] J. T. Stuart, "On finite amplitude oscillations in laminar mixing layers," J. Fluid Mech. **29**, 417 (1967).
[20] J. Watson, "On spatially-growing finite disturbances in plane Poiseuille shear flow," J. Fluid Mech. **14**, 211 (1962).
[21] P. M. Eagles, "On the stability of Taylor vortices by fifth-order amplitude expansions," J. Fluid Mech. **49**, 529 (1972).
[22] J. T. C. Liu, "Finite-amplitude instability of the compressible laminar wake. Weakly nonlinear theory," Phys. Fluids **12**, 1763 (1969).
[23] P. Huerre and P. A. Monkewitz, "Local and global instabilities in spatially developing flows," Annu. Rev. Fluid Mech. **22**, 473 (1990).
[24] M. E. Goldstein and L. S. Hultgren, "Nonlinear spatial evolution of an externally excited instability wave in a free shear layer," J. Fluid Mech. **197**, 295 (1988).
[25] M. E. Goldstein and S. J. Leib, "Nonlinear roll-up of externally excited free shear layers," J. Fluid Mech. **191**, 481 (1988).
[26] H. W. Press, A. S. Teukolsky, T. W. Vetterling, and P. B. Flannery, *Numerical Recipes in FORTRAN* (Cambridge University Press, Cambridge, 1992).
[27] T. F. Balsa and M. E. Goldstein, "On the instabilities of supersonic mixing layers: A high-Mach-number asymptotic theory," J. Fluid Mech. **216**, 585 (1990).
[28] J. T. Stuart, "On the non-linear mechanics of wave disturbances in stable and unstable parallel flows. Part 1. The basic behavior in plane Poiseuille flow," J. Fluid Mech. **9**, 353 (1960).
[29] J. Watson, "On the nonlinear mechanics of wave disturbances in stable and unstable parallel flows. Part 2. The development of a solution for plane Poiseuille flow and for plane Couette flow," J. Fluid Mech. **9**, 371 (1960).
[30] H. Gropengiesser, "On the stability of free shear layers in compressible flows," NASA Technical Report No. TT F-12786, 1969.
[31] S. Ghosh and W. H. Matthaeus, "Low Mach number two-dimensional hydrodynamic turbulence: Energy budget and density fluctuations in a polytropic fluid," Phys. Fluids A **4**, 148 (1992).
[32] F. Ladeinde, E. E. O'Brien, X. Cai, and W. Liu, "Advection by polytropic compressible turbulence," Phys. Fluids **7**, 2848 (1995).